Monthly Notices
of the
ROYAL ASTRONOMICAL SOCIETY

Mon. Not. R. Astron. Soc. **417,** 261–279 (2011) doi:10.1111/j.1365-2966.2011.19128.x

The Type IIP SN 2007od in UGC 12846: from a bright maximum to dust formation in the nebular phase⋆

C. Inserra,[1,2,3]† M. Turatto,[2,4] A. Pastorello,[5] S. Benetti,[6] E. Cappellaro,[6] M. L. Pumo,[6] L. Zampieri,[6] I. Agnoletto,[6] F. Bufano,[6] M. T. Botticella,[6] M. Della Valle,[7] N. Elias Rosa,[8] T. Iijima,[9] S. Spiro[10] and S. Valenti[5]

[1]*Dipartimento di Fisica ed Astronomia, Universitá di Catania, Sezione Astrofisica, Via S.Sofia 78, 95123 Catania, Italy*
[2]*INAF Osservatorio Astrofisico di Catania, Via S.Sofia 78, 95123 Catania, Italy*
[3]*Department of Physics and Astronomy, University of Oklahoma, Norman, OK 73019, USA*
[4]*INAF Osservatorio Astronomico di Trieste, Via Tiepolo 11, 34143 Trieste, Italy*
[5]*Astrophysics Research Centre, School of Mathematics and Physics, Queen's University Belfast, Belfast BT7 1NN*
[6]*INAF Osservatorio Astronomico di Padova, Vicolo dell'Osservatotio 5, 35122 Padova, Italy*
[7]*INAF Osservatorio Astronomico di Capodimonte, Salita Moiariello 16, 80131 Napoli, Italy*
[8]*Institut de Ciències de l'Espai (IEEC-CSIC), Campus UAB, 08193 Bellaterra, Spain*
[9]*INAF Osservatorio Astronomico di Padova, Sezione di Asiago, Osservatorio Astrofisico, 36012 Asiago (Vi), Italy*
[10]*INAF National Institute for Astrophysics, I-00136 Rome, Italy*

Accepted 2011 May 24. Received 2011 May 23; in original form 2011 February 26

ABSTRACT

Ultraviolet, optical and near-infrared observations of the Type IIP supernova (SN) 2007od, covering from maximum light to late phases, allow detailed investigation of different physical phenomena in the expanding ejecta. These data turn this object into one of the most peculiar SNe IIP ever studied. The early light curve of SN 2007od is similar to that of a bright IIP, with a short plateau, a bright peak ($M_V = -18$ mag), but a very faint late-time optical light curve. However, with the inclusion of mid-IR observations during the radioactive tail, we derive an ejected mass of ^{56}Ni of $M(^{56}\mathrm{Ni}) \sim 2 \times 10^{-2}\,\mathrm{M}_\odot$. By modelling the bolometric light curve, ejecta expansion velocities and blackbody temperature, we estimate a total ejected mass of 5–7.5 $\mathrm{M}_\odot$ with a kinetic energy of at least 0.5×10^{51} erg. The early spectra reveal a boxy Hα profile and high-velocity features of the Balmer series that suggest the possible interaction of the ejecta with a close circumstellar matter (CSM). The interaction with the CSM and the presence of dust formed inside the ejecta are evident in the late-time spectra. The episodes of mass-loss shortly before explosion, the bright plateau, the relatively small amount of ^{56}Ni and the faint [O I] emission observed in the nebular spectra are consistent with a super-asymptotic giant branch progenitor ($M \sim 9.7$–$11\,\mathrm{M}_\odot$).

Key words: circumstellar matter – supernovae: general – supernovae: individual: SN 2007od – galaxies: individual: UGC 12846.

1 INTRODUCTION

Type II supernovae (SNe II) are produced in explosions following the gravitational collapse of the cores of massive [zero-age main-sequence (ZAMS) mass $\geq 8\,\mathrm{M}_\odot$] stars that retain part of their H envelopes. SNe II of the subtype called 'plateau' (SNe IIP) show constant luminosity lasting from 30 days to 3–4 months. Other SNe II, presenting a steep linear decline over the same period, are named 'linear' (SNe IIL; Barbon, Ciatti & Rosino 1979). SNe IIP were the subject of extensive analysis by Hamuy (2003) who pointed out a continuum in their properties and revealed several relations between physical parameters. An independent analysis, extending the sample to both low and high luminosities, was performed by Pastorello (2003) who confirmed the above results. These studies show that most sit in the region of $M_{\mathrm{ej}} \approx 12$–$17\,\mathrm{M}_\odot$, regardless of the mass of radioactive ^{56}Ni, and only for relatively large ^{56}Ni masses ($\geq 10^{-2}\,\mathrm{M}_\odot$), M_{ej} increases with M_{Ni}. This suggests a possible

⋆ Based on observations collected at the Italian 3.58-m Telescopio Nazionale Galileo, the Liverpool Telescope and the North Optical Telescope (La Palma, Spain), the Calar Alto Observatory (Sierra de los Filabres, Spain), the orbital Telescope *Swift* and at the Italian Rapid Eye Movement Telescope (La Silla, Chile), and the Copernico and Galileo Galilei telescopes (Asiago, Italy).
†E-mail: cosimo.inserra@oact.inaf.it

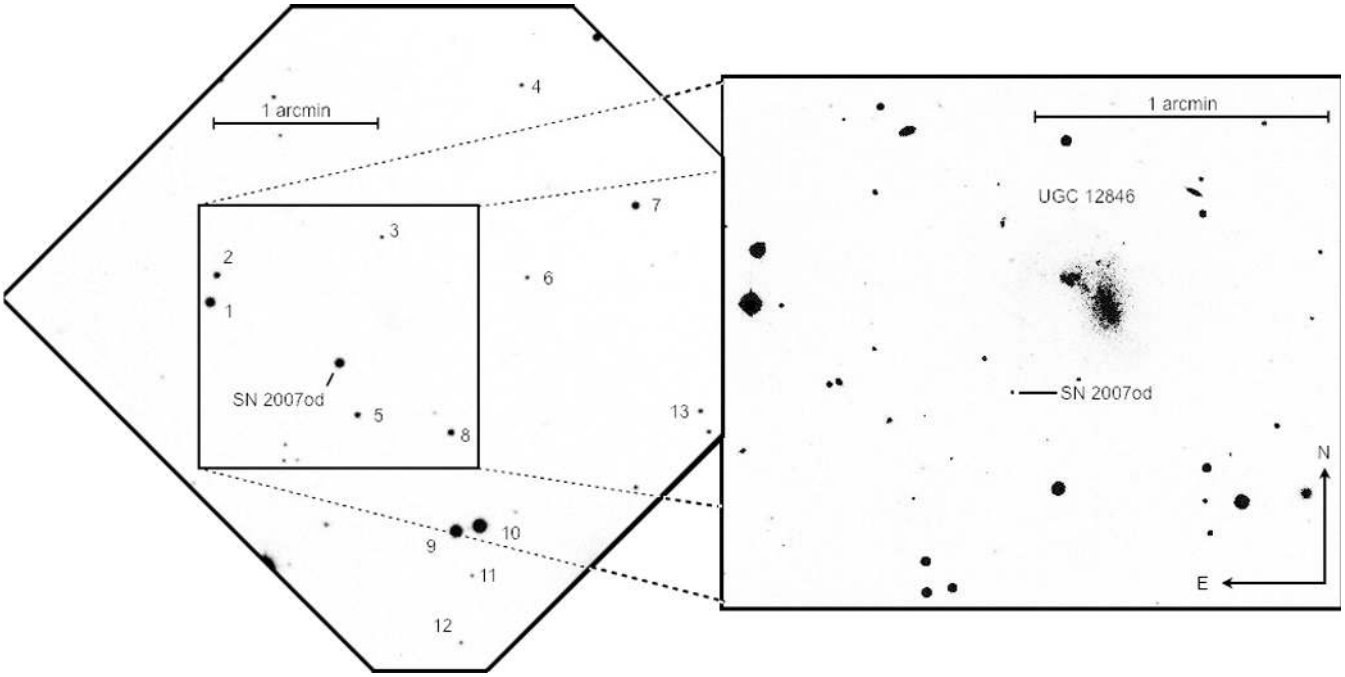

Figure 1. Left: *R*-band image of SN 2007od in UGC 12846 obtained in 2007 November with the 1.82-m Copernico Telescope + AFOSC at Mt. Ekar (Asiago, Italy). The exposure is so short that the LSB parent galaxy is barely visible. The sequence of stars in the field used to calibrate the optical and NIR magnitude of SN 2007od is also labelled. Right: blow-up of the region of the parent galaxy in an *R*-band frame obtained on 2008 July 16 with the 2.2-m Telescope of Calar Alto equipped with CAFOS (see Table 1).

bimodal distribution of $M_{\rm ej}$ versus other observables. Thanks to the direct identification of a few SN precursors in deep pre-explosion images, recent studies indicate that most SNe IIP originate from the explosion of stars with $M \lesssim 15\,{\rm M}_{\odot}$ (Smartt et al. 2009).

Although SNe IIP are possibly the best studied core-collapse explosions, there are several issues that remain unclear, e.g. the nucleosynthesis yields, the nature and rate of the mass-loss in the latest stages of evolution of the precursor [this can affect the optical and radio display once the wind material is overcome by the ejecta; see Moriya et al. (2010) and Smith et al. (2011)], the influence of the metallicity on the progenitor evolution (see Kasen & Woosley 2009) and the location and amount of dust formation and its impact on the observables (see Maguire et al. 2010).

SN 2007od is an ideal test case to address such issues. It was discovered on 2007 November 2.85 UT in the nearby galaxy UGC 12846 (Mikuz & Maticic 2007). Blondin & Calkins (2007) classified it as a normal SN IIP about two weeks after explosion, and reported some similarity with the spectrum of Type II SN 1999em 10 days after explosion. On November 6, the SN was detected by *Swift* with UVOT, although not with XRT (3σ upper limit $<1.4 \times 10^{-13}$ erg cm^{-2} s^{-1}; Immler & Brown 2007).

The coordinates of SN 2007od have been measured on our astrometrically calibrated images at two different epochs: $\alpha = 23^{\rm h}55^{\rm m}48\overset{\rm s}{.}68 \pm 0\overset{\rm s}{.}1$ and $\delta = +18^{\circ}24'54\overset{''}{.}8 \pm 0\overset{''}{.}1$ (J2000). The SN is located in a peripheral region of UGC 12846, 38 arcsec east and 31 arcsec south of the core of the galaxy (Fig. 1). This position, slightly revised with respect to previous determinations (Mikuz & Maticic 2007), corresponds to a linear distance of ∼6 kpc from the nucleus (assuming a distance to UGC 12846 of ∼26 Mpc; cf. Section 2.5). A prior work based on late-time observations of SN 2007od has been done by Andrews et al. (2010).

In this paper, we present optical and near-infrared (NIR) observations of SN 2007od spanning from 2007 November to 2008 September. In Section 2, we describe photometric observations and reduction, estimate the interstellar reddening towards the SN site and describe the photometric evolution. In Section 3 we analyse the spectroscopic data. In Section 4 we provide evidence for dust formation in SN 2007od. Discussion and conclusions follow in Sections 5 and 6, respectively.

2 PHOTOMETRY

The optical and NIR photometric follow-up of SN 2007od began on 2007 November 6, four days after the discovery, and lasted until late 2008 February. Observations were resumed in 2008 June after the seasonal gap.

2.1 Optical ground-based data

Optical (*UBVRI*) photometry was obtained using a number of ground-based telescopes (Table 1). Note that the *i*-band filter used at the 2.56-m Nordic Optical Telescope (NOT) on 2008 January 13 is an interference filter with central wavelength (7970 Å), slightly different from the classical Gunn or Cousins *I* and more similar to Sloan *i*. In our analysis, however, it was calibrated as Cousins *I*.

Optical data were reduced following standard prescriptions in IRAF[1] environment. Instrumental magnitudes were measured on the images obtained after removal of the detector signature (overscan, bias and flat-field corrections, and trimming).

[1] Image Reduction and Analysis Facility, distributed by the National Optical Astronomy Observatories, which are operated by the Association of Universities for Research in Astronomy, Inc., under contract to the National Science Foundation.

Table 1. Instrumental configurations used for the photometric follow-up.

Telescope	Primary mirror (m)	Camera	Array	CCD	Pixel scale (arcsec pixel^{-1})	Field of view (arcmin)	Filters
Copernico	1.82	AFOSC	1024 × 1024	TK1024AB	0.46	8.1	Bessell *B V R*, Gunn *i*
TNG	3.58	DOLORES[a]	2048 × 2048	EEV 42-40	0.25	8.6	Johnson *U B V*, Cousins *R I*
		NICS	1024 × 1024	HgCdTe Hawaii	0.25	4.2	*J H K*
REM	0.60	ROSS	1024 × 1024	Apogee Alta	0.575	10	Johnson *V*, Cousins *R I*
		REMIR	512 × 512	Hawaii I	1.2	10	*J H K*
LT	2.0	RATcam	2048 × 2048	EEV 42-40	0.13	4.6	Sloan *u*, Bessell *B V*
NOT	2.5	ALFOSC	2048 × 2048	EEV 42-40	0.19	6.4	Johnson *U B V R*, interference *i*
CAHA	2.2	CAFOS	2048 × 2048	SITe	0.53	16	Johnson *B V R I*
Swift	0.3	UVOT	2048 × 2048	Microchannel Intensified CCD	0.48	17	*uvw2*, *uvm2*, *uvw1*,*u*, *b*, *v*

Notes. Copernico = Copernico Telescope (Mt. Ekar, Asiago, Italy); TNG = Telescopio Nazionale Galileo (La Palma, Spain); REM = Rapid Eye Mount Telescope (La Silla, Chile); LT = Liverpool Telescope (La Palma, Spain); NOT = Nordic Optical Telescope (La Palma, Spain); CAHA = Calar Alto Observatory (Sierra de los Filabres, Andalucia, Spain); *Swift* by NASA. [a]Observations from 2007 November 1 to December 31 were performed with an engineering CCD with the same general characteristics.

Table 2. Magnitudes of the local sequence stars in the field of SN 2007od (cf. Fig. 1). The rms values of the measurements are in brackets.

ID	*U*	*B*	*V*	*R*	*I*
1	15.254 (.025)	15.206 (.026)	14.436 (.020)	13.994 (.019)	13.697 (.017)
2	17.933 (.008)	17.035 (.011)	15.947 (.021)	15.335 (.017)	14.859 (.021)
3	18.831 (.018)	18.238 (.010)	17.264 (.026)	16.798 (.033)	16.291 (.023)
4		17.833 (–)	17.002 (.034)	16.542 (.044)	15.942 (.014)
5	18.576 (.041)	17.540 (.022)	16.426 (.018)	15.764 (.021)	15.228 (.022)
6	18.338 (.046)	18.264 (.029)	17.102 (.025)	16.803 (.021)	16.295 (.027)
7	15.612 (–)	15.770 (.055)	15.106 (.023)	14.819 (.029)	14.373 (.020)
8	18.351 (.009)	17.324 (.018)	16.122 (.024)	15.438 (.020)	14.760 (.021)
9	15.501 (.020)	14.583 (.003)	13.452 (.020)	12.834 (.017)	12.192 (.016)
10	14.584 (.027)	13.845 (.006)	12.858 (.017)	12.304 (.019)	11.743 (.018)
11	18.522 (.011)	18.271 (.031)	17.463 (.026)	17.090 (.029)	16.608 (.014)
12	17.748 (–)	17.955 (.030)	17.309 (.042)	17.058 (.031)	16.644 (.022)
13		17.926 (–)	16.777 (.040)	16.079 (.013)	16.005 (.002)

Photometric zero-points and colour terms were computed for all nights through observations of Landolt standard fields (Landolt 1992). 11 out of 28 nights turned out to be photometric. Using these nights we calibrated the average magnitudes of the local sequence stars shown in Fig. 1. Magnitudes are reported in Table 2 along with their rms (in brackets). For stars in common with Andrews et al. (2010), the magnitudes differ on average by $\Delta B \sim 0.07 \pm 0.02$, $\Delta V \sim 0.03 \pm 0.02$, $\Delta R \sim 0.05 \pm 0.01$, $\Delta I \sim 0.03 \pm 0.02$. These differences are probably related to the uncertainties in the transformation to the Johnson–Cousins system adopted in Andrews et al. (2010). Eventually, the local sequence stars were used to calibrate the photometric zero-points obtained in the non-photometric nights.

Calibrated optical magnitudes of the SN are reported in Table 3 along with early magnitudes from Mikuz & Maticic (2007). There is no evidence of the SN in images obtained on 2008 September 17, and the values reported are the limiting magnitudes computed by placing artificial stars near the position of the SN.

SN magnitudes were measured by means of the point spread function (PSF) fitting technique. The adoption of the PSF technique is justified by the occurrence of the SN in the outskirts of the parent galaxy, in a region with a smooth background. The uncertainties reported in Table 3 were estimated by combining in quadrature the errors of the photometric calibration and the errors of the PSF fitting through artificial stars.

Optical observations with the 0.6-m Rapid Eye Mount (REM) telescope plus ROSS were affected by random deformations of the PSF. For this reason the SN magnitudes were always determined with aperture photometry with respect to a few local sequence stars close to SN. REM observations at airmasses >2 were rejected, because the star shapes on the frames were elliptical and neither this approach nor PSF fitting produced consistent measurements.

2.2 NIR data

NIR photometry (*JHK*) was obtained with NICS mounted at the 3.5-m Telescopio Nazionale Galileo (TNG) and with REMIR at REM (cf. Table 1). The reduction of NIR images included the subtraction of sky images obtained by combining several dithered exposures. Then NIR images of the SN field for each band were obtained by combining several sky-subtracted, dithered exposures. Photometric calibration was achieved relative to Two Micron All Sky Survey (2MASS) photometry of the same local sequence stars used for the calibration of the optical photometry. The NIR magnitudes of SN 2007od are listed in Table 4. The values reported for the *K* band of NICS were obtained with the K' filter, instead.

Table 3. Ground-based *UBVRI* magnitudes of SN 2007od and assigned errors (in brackets).

Date dd/mm/yy	JD (+240 0000)	*U*	*B*	*V*	*R*	*I*	Inst.
02/11/07	54407.35				14.4 (–)		7
03/11/07	54408.30		14.5 (–)		13.9 (–)		7
06/11/07	54411.57			14.144 (.025)	13.945 (.022)	13.821 (.024)	2
08/11/07	54413.21		14.464 (.028)	14.263 (.026)	13.991 (.021)	13.873 (.023)	1
09/11/07	54413.62			14.350 (.027)	14.095 (.025)	13.893 (.028)	2
12/11/07	54416.64			14.392 (.032)	14.148 (.028)	13.846 (.024)	2
12/11/07	54417.42		14.655 (.029)	14.329 (.025)	14.084 (.021)	14.009 (.022)	1
16/11/07	54421.43	14.353 (.033)	14.902 (.027)	14.486 (.031)	14.069 (.028)	13.913 (.023)	3
16/11/07	54421.54			14.415 (.027)	14.107 (.025)	13.606 (.024)	2
21/11/07	54425.53			14.474 (.050)	14.132 (.042)	13.886 (.031)	2
24/11/07	54428.58			14.535 (.046)	14.135 (.050)	13.930 (.055)	2
27/11/07	54432.54			14.558 (.028)	14.186 (.027)	13.971 (.025)	2
01/12/07	54435.56			14.533 (.028)	14.194 (.026)	13.960 (.025)	2
05/12/07	54439.34		15.503 (.034)	14.707 (.025)	14.198 (.023)	13.980 (.022)	1
06/12/07	54441.35	15.868 (.036)	15.570 (.030)	14.780 (.025)			4
07/12/07	54441.55			14.709 (.034)	14.249 (.029)	13.967 (.025)	2
11/12/07	54445.55			14.764 (.034)	14.288 (.028)	14.108 (.025)	2
15/12/07	54450.34	16.308 (.038)	15.784 (.028)	14.803 (.025)			4
15/12/07	54450.45	16.198 (.038)	15.805 (.026)	14.756 (.025)	14.367 (.021)	14.228 (.025)	3
21/12/07	54455.55			14.870 (.085)	14.452 (.021)	14.440 (.029)	2
25/12/07	54459.53			14.975 (.127)	14.522 (.028)	14.217 (.029)	2
25/12/07	54460.33	16.833 (.038)	16.022 (.028)	15.006 (.028)			4
28/12/07	54462.20		16.228 (.028)	15.096 (.027)	14.574 (.023)	14.366 (.022)	1
29/12/07	54463.53			15.023 (.062)	14.454 (.028)	14.234 (.024)	2
13/01/08	54479.36	17.509 (.044)	16.622 (.027)	15.350 (.025)	14.688 (.022)	14.589 (.021)	6
28/01/08	54494.26		17.184 (.029)	15.724 (.028)	14.871 (.023)	15.011 (.023)	1
17/02/08	54514.25			16.926 (.032)	16.197 (.025)	15.983 (.028)	1
05/07/08	54653.62		22.392 (.197)	21.714 (.164)	20.748 (.058)	20.882 (.264)	5
16/07/08	54664.62			21.987 (.101)	21.057 (.064)		5
04/09/08	54714.59			22.330 (.057)	21.564 (.028)	21.314 (.032)	3
17/09/08	54727.42			> 22.0	> 21.2	> 21.2	5

Notes. 1 = Copernico, 2 = REM, 3 = TNG, 4 = LT, 5 = CAHA, 6 = NOT, 7 = CBET 1116. Telescope abbreviations are the same as in Table 1. Unfiltered photometry from CBET 1116 is considered most similar to the *R*-band Johnson–Bessell system.

Table 4. *JHK* magnitudes of SN 2007od and assigned errors (in brackets). We accounted for both measurement errors and uncertainties in the photometric calibration.

Date dd/mm/yy	JD (+240 0000)	*J*	*H*	*K*	Inst.
06/11/07	54410.57	13.712 (.045)	13.602 (.070)		2
09/11/07	54413.62		13.628 (.044)	13.804 (.089)	2
12/11/07	54416.64	13.748 (.036)	13.625 (.048)		2
16/11/07	54421.54	13.725 (.046)	13.649 (.041)	13.592 (.122)	2
21/11/07	54425.53	13.820 (.024)	13.641 (.023)	13.697 (.083)	2
24/11/07	54428.58		13.642 (.041)	13.612 (.062)	2
27/11/07	54432.54	13.792 (.019)	13.641 (.025)	13.653 (.048)	2
01/12/07	54435.56	13.841 (.018)	13.571 (.046)	13.559 (.054)	2
07/12/07	54441.55	13.798 (.042)			2
11/12/07	54445.55	13.851 (.029)	13.628 (.021)	13.598 (.069)	2
21/12/07	54455.55	13.836 (.035)	13.613 (.031)	13.584 (.062)	2
25/12/07	54459.53	13.789 (.045)	13.694 (.044)	13.942 (.130)	2
29/12/07	54463.53	13.941 (.019)	13.765 (.039)	13.773 (.067)	2
12/01/08	54478.31	14.333 (.037)	14.233 (.039)	13.901 (.029)	3
11/06/08	54629.73	19.612 (.029)	19.300 (.047)		3

Notes. 2 = REM, 3 = TNG (K' filter). The abbreviations and the numbers are the same as in Table 1.

2.3 *Swift* data

For SN 2007od a number of optical and UV observations, obtained by UVOT on-board the *Swift* satellite, are available. UVOT data were obtained in *uvw2*, *uvm2*, *uvw1*, *u*, *b*, *v* filters (Poole et al. 2008) with spatial resolution of about 2 arcsec (full width at half-maximum, FWHM).

12 epochs of observations, spread over a period of about 60 days, are available along with two late-time observations at about 300 days when the SN was below the detection threshold. We reduced

Table 5. *Swift* magnitudes of SN 2007od and assigned errors (in brackets). The *UBV* magnitudes have been corrected for the small systematic differences mentioned in the text.

Date dd/mm/yy	JD (+240 0000)	*uvw2*	*uvm2*	*uvw1*	*U*	*B*	*V*
04/11/07	54409.50	14.68 (.05)	14.52 (.06)	14.15 (.06)	13.49 (.04)	14.34 (.06)	14.19 (.04)
07/11/07	54411.52	14.90 (.05)	14.74 (.06)	14.36 (.05)	13.66 (.05)	14.41 (.05)	14.22 (.04)
09/11/07	54413.78	15.32 (.06)	15.20 (.06)				
11/11/07	54415.79	15.70 (.05)	15.54 (.06)	15.03 (.06)	14.11 (.05)	14.60 (.05)	14.35 (.04)
13/11/07	54417.80	16.13 (.06)	16.00 (.06)	15.37 (.06)	14.30 (.05)	14.68 (.05)	14.36 (.04)
17/11/07	54421.88	15.97 (.03)	16.74 (.07)	15.97 (.07)	14.90 (05)	14.90 (.05)	14.41 (.04)
23/11/07	54427.83	17.63 (.07)	17.63 (.08)	16.69 (.07)	15.40 (.05)	15.24 (.05)	14.59 (.04)
04/12/07	54438.55	18.31 (.08)	18.25 (.11)	17.28 (.08)	15.78 (.05)	15.56 (.05)	14.71 (.04)
14/12/07	54448.52	18.76 (.11)	18.92 (.13)	17.69 (.08)	16.20 (.06)	15.74 (.05)	14.84 (04)
07/01/08	54473.16	19.58 (.13)	19.69 (.22)	18.33 (.10)	17.33 (.07)	16.38 (.05)	15.25 (.04)
04/08/08	54683.02	> 20.9			> 20.9	> 21.2	> 20.2
23/08/08	54701.96	> 20.4	>19.6	> 21.3	> 21.0	> 21.0	> 20.2

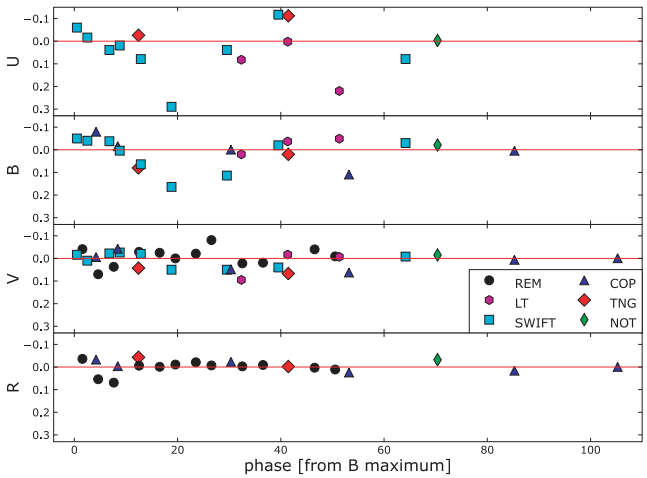

Figure 2. *U*-, *B*-, *V*- and *R*-band residuals in the first 106 days with respect to low-order polynomial fits of all available data. Different instruments are marked with different symbols.

these data using HEASARC[2] software. All images for each epoch were first co-added, then reduced following the guidelines of Poole et al. (2008). Aperture magnitudes were transformed from the *Swift* system to Johnson magnitudes through the colour transformations of Li et al. (2006). By comparing the space and the ground-based SN magnitudes at corresponding epochs, we found an average difference (ground–space) $\Delta U \sim 0.19 \pm 0.03$, $\Delta B \sim 0.04 \pm 0.03$ and $\Delta V \sim 0.09 \pm 0.03$. These corrections have been applied to all UVOT magnitudes, and the resulting magnitude values are reported in Table 5.

To check for possible biases due to the peculiar passbands of UVOT (and other instruments), in Fig. 2 we show the residuals with respect to a low-order polynomial fit of all the available values. The agreement of the ground-based data is overall good with few measurements deviating by more than 0.05 mag. *Swift* data deviate more. The largest differences are for the *U* band in which the specific detector responses and the variable transmission at atmospheric cut-off can generate quite different passbands.

[2] NASA's High Energy Astrophysics Science Archive Research Center.

2.4 Photometric evolution

uvw2, *uvm2*, *uvw1*, *U*, *B*, *V*, *R*, *I*, *J*, *H* and *K* light curves of SN 2007od are plotted in Fig. 3. This figure includes also photometric data from Andrews et al. (2010). As stressed by these authors, the *F606W* and the Gemini *r* filters (transformed respectively to the *V* and *R*) include the Hα line, and care should be taken when comparing these data with standard photometry of other SNe. Both in the photospheric and in the nebular phases, the data of Andrews et al. (2010) are in good agreement with our data (cf. Section 2.1).

The *R*-band light curve shows a fast rise to the peak, estimated to occur around JD 245 4409.0±2.0. In fact, early unfiltered observations from Mikuz & Maticic (2007) showed that the SN was still rising to the *R*-band maximum at discovery (November 2.85 UT). This is also consistent with the phases derived for the first spectra of SN 2007od through a cross-correlation with a library of SN spectra performed with the 'GELATO' code (Harutyunyan et al. 2008). Therefore, hereafter we will adopt JD 2454 404±5 (October 30.5 UT) as an estimate for the epoch of shock breakout.

In Figs 3 and 4, an early (short) post-peak decline is visible mainly in the *BVR* bands, while the *U* band shows a monotonic decline.

A short, flat plateau is visible at longer wavelengths with $m_R \sim 14.3$ ($M_R \sim -17.8$; cf. Section 2.5) between about day 15 and day 45. The plateau of SN 2007od is, therefore, relatively luminous when compared with that of more typical SNe IIP (Patat et al. 1994; Richardson et al. 2002) and similar to those of SNe 1992H (Clocchiatti et al. 1996) and 2004et (Kotak et al. 2009; Maguire et al. 2010).

The SN was recovered about 240 days after maximum light. Unfortunately, our observations do not cover the plateau-tail transition which would allow interesting diagnostics for the explosion parameters (Elmhamdi, Chugai & Danziger 2003a). It is remarkable that from the plateau to the first point of the radioactive tail there is a drop of ∼6 mag in about 200 days, which is much larger than that seen in normal SNe IIP. Afterwards, the late-time decline rates in the different bands (cf. Table 10), computed including also data from Andrews et al. (2010), are rather similar to those of most normal SNe IIP (Turatto et al. 1990; Patat et al. 1994). The *V* band decline rate is 0.94 mag $(100\,\mathrm{d})^{-1}$, close to the 0.98 mag $(100\,\mathrm{d})^{-1}$ (e-folding time 111.26 d) expected if the luminosity is powered by the decay of ^{56}Co to ^{56}Fe.

In Fig. 5 we show the time evolution of $B-V, V-I$ and $J-H$ colour curves of SN 2007od, together with those of SNe 1987A, 2005cs, 2004et, 1999em, dereddened according to the values of

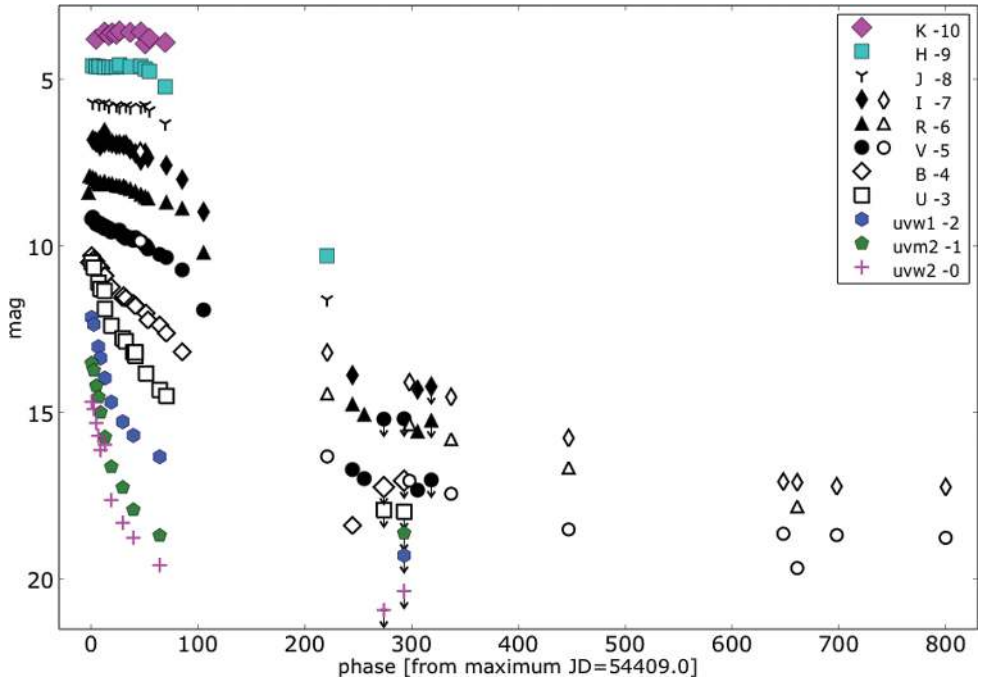

Figure 3. Synoptic view of the light curves of SN 2007od in all available bands. *U*, *B* and *V* light curves include data both from ground-based telescopes (Table 1) and *Swift* (see Section 2.3); *RIJHK* light curves from ground-based telescope images; and *uvw2*, *uvm2* and *uvw1* light curves only from *Swift*. The magnitude shifts from the original value reported on Table 3 are in the legend. Open *VRI* symbols are magnitude values reported in Andrews et al. (2010).

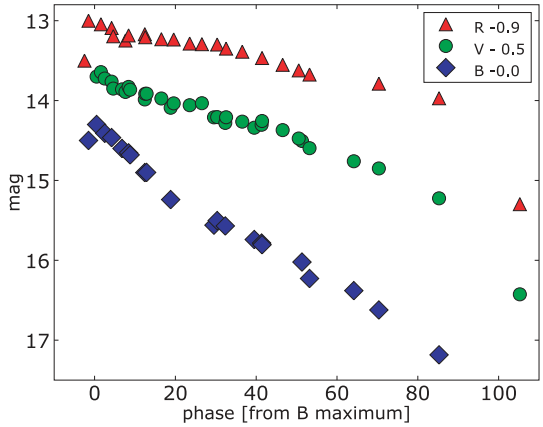

Figure 4. *BVR* light curves in the first four months of the evolution of SN 2007od.

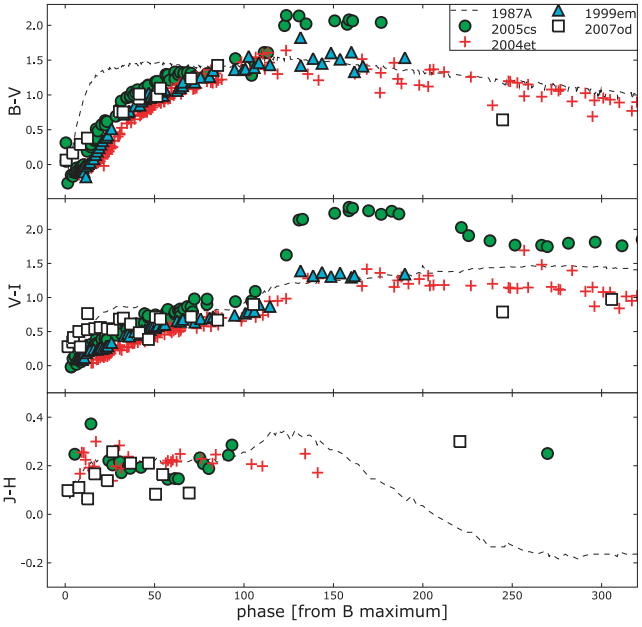

Figure 5. Comparison between the dereddened colours of SN 2007od and those of SNe 1987A, 2005cs, 1999em, 2004et. The phase of SN 1987A is with respect to the explosion date.

Table 6. All these SNe IIP show quite similar colour evolutions with a rapid increase of the $B - V$ colour as the SN envelope expands and cools down. After about 40 days the colour varies more slowly as the rate of cooling decreases. SN 2007od follows this behaviour. The only exception to this smooth trend is SN 2005cs which shows a red spike at about 120 days (when data of SN 2007od are missing). Such a red spike seems to mark low-luminosity SNe IIP in correspondence to the steep post-plateau decline (Pastorello et al. 2004). The $V - I$ colour increases in a linear fashion for all SNe IIP during the plateau phase, and remains roughly constant during the nebular phase (Fig. 5). The colour evolution of SN 2007od is similar to that of other Type IIP SNe, although it is possibly redder at early phases. In the nebular phase, the colour curves of SN 2007od seem to become bluer, especially the $B - V$ curve, similarly to SN 2004et. Note, however, that such claim is based on a single point affected by large uncertainty. The similarity with 2004et in the nebular phase is supported by the $V - I$ colour evolution. Only sparse data are available for Type IIP SNe in the NIR, especially during the nebular phase. For this reason, in this domain we compared only a few well-studied, recent events such as SNe 2005cs and 2004et, plus the reference Type II SN 1987A. Their $J - H$ colour curves (Fig. 5) remain constant at $J - H \approx 0.2$ mag until the phase of ~ 120 d. For the later nebular phase, the single epoch $J - H$ measurement of SN 2007od was found consistent with a similar measurement for SN 2005cs.

Table 6. Main parameters of Type II SNe used in the comparisons with SN 2007od.

SN	μ	$E(B-V)$	Parent galaxy	References
1979C	31.16	0.009	NGC 4321	1
1987A	18.49	0.195	LMC	2
1992H	32.28	0.027	NGC 5377	3
1999em	29.47	0.1	NGC 1637	4, 5
2004et	28.85	0.41	NGC 6946	6
2005cs	29.62	0.05	M 51	7

References. (1) Balinskaia, Bychkov & Neizvestnyi (1980), (2) Arnett et al. (1989), (3) Clocchiatti et al. (1996), (4) Elmhamdi et al. (2003b), (5) Baron et al. (2000), (6) Maguire et al. (2010) and (7) Pastorello et al. (2009).

2.5 Reddening and absolute magnitude

The Galactic reddening to UGC 12846 was estimated as $E_g(B-V) = 0.038$ [$A_g(B) = 0.155$; Schlegel, Finkbeiner & Davis 1998]. In our best resolution optical spectra (cf. Section 3), the absorption features due to interstellar NaID ($\lambda\lambda$5890, 5896) lines of the Galaxy are present with average EW$_g$(NaID) $\sim$ 0.42 Å. According to Turatto, Benetti & Cappellaro (2003), this corresponds to a galactic reddening $E_g(B-V) \sim 0.07$ mag [which can be transformed through the standard reddening law of Cardelli, Clayton & Mathis (1989) to $A_g(B)\sim$0.28]. Interstellar NaID lines at the redshift of UGC 12846 are not detected even in our best signal-to-noise ratio (S/N) NTT spectrum of November 27 [EW$_i$(NaID)$<$ 0.10 Å], suggesting that the extinction in the host galaxy is negligible. This is not surprising, considering the position of the SN well outside the main body of the galaxy, and the absence of foreground/background structure at its location even in our late, deep images. Throughout this paper, therefore, for SN 2007od we will assume a total reddening of $E_g(B-V) = 0.038$ mag.

The NASA/IPAC Extragalactic Data base (NED) provides a heliocentric radial velocity of v_{hel}(UGC 12846) = 1734 $\pm$ 3 km s^{-1}. Correcting for the Virgo infall (V_{Virgo} = 1873 $\pm$ 17km s^{-1}; Mould et al. 2000) and adopting $H_0 = 72$ km s^{-1}Mpc^{-1}, we obtain a distance modulus $\mu = 32.05 \pm 0.15$, which will be used throughout this paper. This is in agreement with the distance modulus μ = 31.91 ($H_0 = 75$ km s^{-1}Mpc^{-1}) provided by Tully (1988). NED provides also the recession velocities corrected for the Virgo cluster, the Great Attractor and the Shapley Supercluster velocity fields (Virgo+GA and Virgo+GA+Shapley). Both are marginally lower and their use would produce distance moduli smaller (and absolute magnitudes fainter) by about 0.1 mag.

Assuming the above distance and extinction values, we find $M_U^{max} = -18.7 \pm 0.18$, $M_B^{max} = -17.8 \pm 0.18$, $M_V^{max} = -18.0 \pm 0.23$, $M_R^{max} = -18.1 \pm 0.21$ and $M_I^{max} = -18.2 \pm 0.23$, where the reported errors include the uncertainties of our photometry, the adopted distance modulus and the interstellar reddening.

2.6 Bolometric light curve and ^{56}Ni mass

The (*uvoir*) bolometric light curve of SN 2007od (Fig. 6) was obtained by converting the observed broad-band magnitudes (*uw2*, *um2*, *uw1*, *U*, *B*, *V*, *R*, *I*, *J*, *H*, *K*) into fluxes at the effective wavelength, then correcting for the adopted extinction (cf. Section 2.5), and finally integrating the resulting spectral energy distribution (SED) over wavelength, assuming zero flux at the integration limits. Flux was then converted to luminosity by using the distance adopted in Section 2.5. The emitted flux was computed at the phases in which

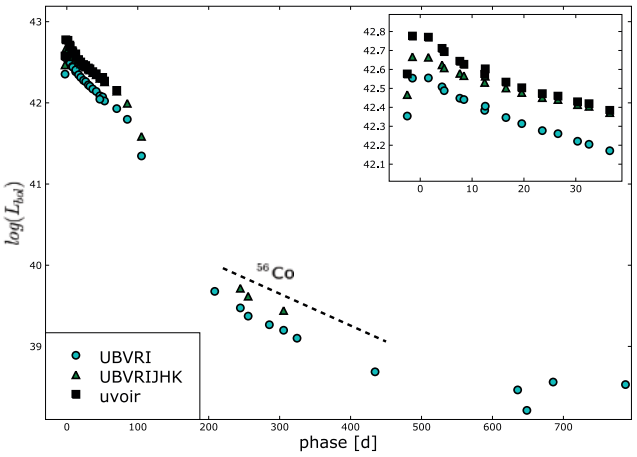

Figure 6. *uvoir* (black squares), *UBVRIJHK* (green triangles) and *UBVRI* (cyan circles) light curves of SN 2007od. Also reported is the extension of the *UBVRI* light curve to late phases obtained with data of Andrews et al. (2010). The slope of ^{56}Co to ^{56}Fe decay is also displayed for comparison. A blow-up until 40-d post maximum is shown in the upper-right corner. Distance modulus and reddening are those reported in Table 10.

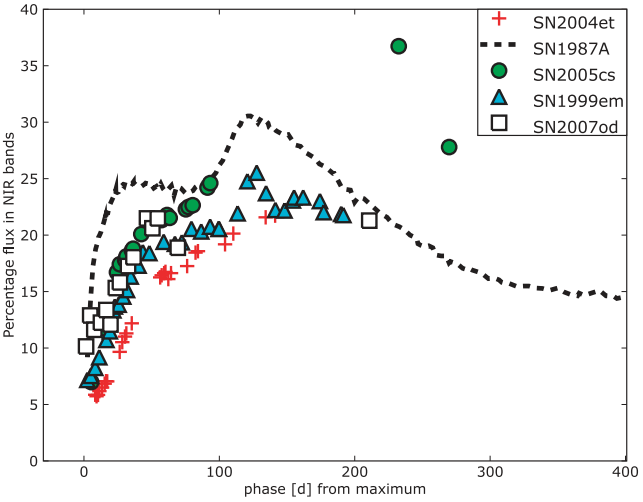

Figure 7. Flux contribution of NIR bands to the *U*-to-*K* bolometric light curve for a sample of SNe IIP.

R observations were available. When observations in a bandpass were unavailable in a given night, the magnitudes were obtained by interpolating the light curves using low-order polynomials, or were extrapolated using constant colours. The pre-maximum bolometric is based mainly on *R*-band observations and should be regarded as uncertain. The peak of the *uvoir* bolometric light curve is reached very close in time to the *R* maximum, on JD$_{max}^{bol}$ = 245 4410.0 $\pm$ 2.0, and at a luminosity $L_{bol} = 6.0 \times 10^{42}$ erg s^{-1}. In Fig. 6, together with the *uvoir* light curve, we also plot the light curves obtained by integrating *UBVRI* and *UBVRIJHK* contributions only.

The light curve (from *U* to *K*) of SN 2007od shows a significant NIR (*JHK*) contribution, as displayed in Fig. 7. The progressive rise of the NIR flux in the photospheric phase is similar to that of other SNe IIP, while the contribution in the nebular phase is constant at least until $\sim$220 d (Fig. 7). This result is similar to that found by Maguire et al. (2010) for SN 2004et.

As for individual bands, the nebular tail of the bolometric light curve closely matches the slope expected from the decay of ^{56}Co

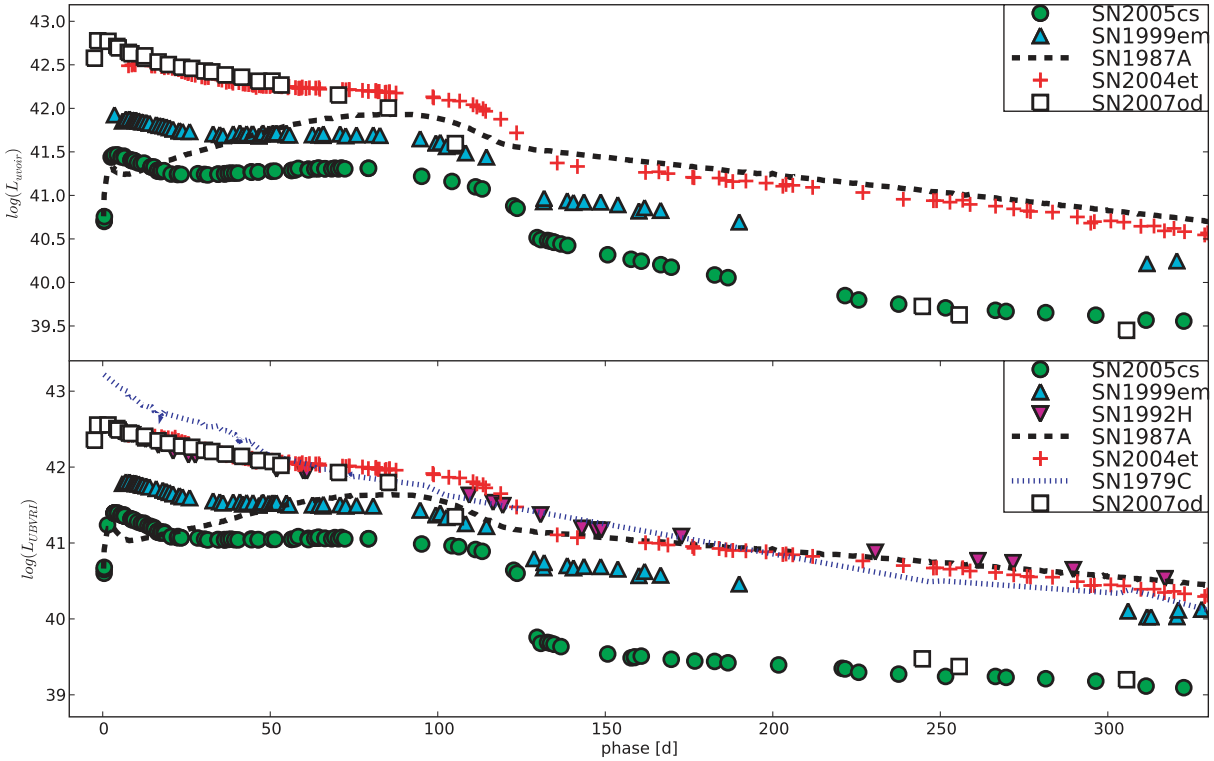

Figure 8. Comparison of quasi-bolometric light curves of SN 2007od with those of other Type II SNe. The comparison on the whole optical-to-NIR (*UBVRIJHK*) domain is in the top panel, while that on the *UBVRI* range is in the bottom panel. For SN 1992H the data are limited to *BVR*, while for SN 1979C are *UBVR*. The distances and reddenings adopted for the comparison with our SN sample are reported in Table 6. Minor misalignments in the epoch of maxima are due to the different epochs adopted for the maxima of the reference band light curve and the quasi-bolometric curve.

to ^{56}Fe, suggesting complete γ-ray trapping. The measured slope is $\gamma \sim 1.053$ mag 100 d^{-1}, close to the canonical value of $\gamma \sim 0.98$ mag 100 d^{-1} of ^{56}Co decay. After day 500, the curve, based only on data by Andrews et al. (2010), flattens.

In Fig. 8, we compare the bolometric light curve of SN 2007od with those of other SNe. The comparison points out the large drop in magnitude (∼6 mag) from the plateau to the radioactive tail and the small amount of ^{56}Ni (cf. Section 4). The SNe chosen for the comparison are those reported in Table 6. Unfortunately, not many of them have spectral coverage from the optical to the NIR, and therefore the comparison was done either for *UBVRIJHK* (top panel) or *UBVRI* (bottom panel) bolometric curves. The early luminosity of SN 2007od is comparable to those of the luminous SN 1992H and SN 2004et. The behaviour of the light curve is certainly more similar to that of Type IIP SNe with respect to the linear SN II 1979C proposed for comparison [the average decline rate by Patat et al. (1994) is β^{B}_{100}(07od) ∼ 3.2 mag (100 d)$^{-1}$, typical of SN IIP]. The similarity to SN 1992H is noticeable in the photospheric phase where both SNe present the same early decline and short plateau, a possible evidence of a low-mass H envelope. On the other hand, the radioactive tail of SN 2007od is more than 1 dex fainter than that of SN 1992H.

The ^{56}Ni mass ejected in the nebular phase by SN 2007od can be derived by comparing the bolometric light curve (Fig. 8, top) to that of SN 1987A assuming a similar γ-ray deposition fraction:

$$M(^{56}\mathrm{Ni})_{07\mathrm{od}} = M(^{56}\mathrm{Ni})_{87\mathrm{A}} \times \frac{L_{07\mathrm{od}}}{L_{87\mathrm{A}}}\,\mathrm{M}_{\odot}, \quad (1)$$

where $M(^{56}\mathrm{Ni})_{87\mathrm{A}} = 0.075 \pm 0.005\,\mathrm{M}_{\odot}$ is the mass of ^{56}Ni ejected by SN 1987A (Arnett 1996), and $L_{87\mathrm{A}}$ is the bolometric luminosity at comparable epoch. The comparison gives $M(^{56}\mathrm{Ni})_{07\mathrm{od}} \sim 0.003\,\mathrm{M}_{\odot}$. Making the reasonable assumption that γ-rays from ^{56}Co decay are fully thermalized at this epoch, we cross-checked this result with the formula:

$$M(^{56}\mathrm{Ni})_{07\mathrm{od}} = \left(7.866 \times 10^{-44}\right) L_t \exp\left[\frac{(t - t_0)/(1+z) - 6.1}{111.26}\right] \mathrm{M}_{\odot} \quad (2)$$

from Hamuy (2003), where t_0 is the explosion epoch, 6.1 d is the half-life of ^{56}Ni and 111.26 d is the e-folding time of the ^{56}Co decay, which releases 1.71 and 3.57 MeV, respectively, as γ-rays (Woosley, Hartmann & Pinto 1989; Cappellaro et al. 1997). This method provides $M(^{56}\mathrm{Ni}) \sim 0.003\,\mathrm{M}_{\odot}$, fully consistent with the previous estimate. Indeed Fig. 8 also shows that $\mathrm{L}_{07\mathrm{od}}$ is similar to that of SN 2005cs, which ejected ∼0.003 $\mathrm{M}_{\odot}$ ^{56}Ni (Pastorello et al. 2009), and to other underluminous Type II events (Pastorello et al. 2004).

The luminous plateau of SN 2007od, comparable with that of the brightest SNe IIP, coupled to an underluminous tail is very unusual (Pastorello 2003). In Section 3.2 we will show that on day 310 (but also in the spectra on day 226 by Andrews et al. 2010) there is evidence of dust formation. Thus the low luminosity in the nebular phase may be due not only to a low ^{56}Ni production. The value determined above should be considered as a lower limit. Indeed, the late-time mid-IR (MIR) data published from Andrews et al. (2010) allow us to study the SED up to the *M* band. The IR bands show clear evidence of strong blackbody emission due to the re-emission of radiation absorbed at shorter wavelengths. Adding this contribution to the bolometric flux, equation (2) provides $M(^{56}\mathrm{Ni})_{07\mathrm{od}} \sim 0.02\,\mathrm{M}_{\odot}$ at the first two epochs of MIR observations. The estimate on a third epoch is less reliable because it is based only on 3.6μ and 4.5μ observations. We address the issue of dust formation in Section 5.

Table 7. Journal of spectroscopic observations of SN 2007od.

Date	JD +240 0000	Phase[a] (d)	Instrumental set-up[b]	Range (Å)	Resolution[c] (Å)
04/11/07	54409.5	5.5	TNG+DOLORES+LRB[d]	3330–7700	14
07/11/07	54412.5	8.5	Pennar+B&C+300tr/mm	3520–8230	10
08/11/07	54413.2	9.2	Copernico+AFOSC+gm4	3500–7820	24
12/11/07	54417.4	13.4	Copernico +AFOSC+gm4,gm2	3640–9150	39
16/11/07	54421.4	17.4	TNG+DOLORES+LRB,LRR[d]	3280–9190	14
27/11/07	54431.5	27.5	NTT+EMMI+gm2,gr5	3200–9710	11
05/12/07	54439.4	35.4	Copernico +AFOSC+gm4,gm2	3660–9160	25
15/12/07	54450.4	46.4	TNG+DOLORES+LRB,LRR[d]	3400–9100	14
28/12/07	54463.2	59.2	Copernico +AFOSC+gm4,gm2	3780–9150	23
13/01/08	54479.4	75.4	NOT+ALFOSC+gm4	3600–9120	13
28/01/08	54494.3	90.3	Copernico +AFOSC+gm4	3640–7760	23
05/09/08	54714.5	311	TNG+DOLORES+LRR	5050–10 250	16
02/10/08	54741.7	338	PALOMAR+DBSP+red	5800–9270	17

[a]With respect to the explosion epoch (JD 245 4404). [b]The abbreviations are the same as in Table 1 with, in addition, Pennar = 1.22-m Galileo Galilei telescope (Pennar, Asiago, Italy) and PALOMAR = 5.1-m Hale Telescope (San Diego County, California, U.S.A.). [c]As measured from the FWHM of the night sky lines. [d]Engineering CCD.

3 SPECTROSCOPY

The spectroscopic monitoring of SN 2007od was carried out with several telescopes over a period of 11 months. The journal of spectroscopic observations is reported in Table 7.

3.1 Spectra reduction

Spectra were reduced (trim, overscan, bias and flat-field corrected) using standard routines of IRAF. Optimal extraction of the spectra was implemented to improve the S/N. Wavelength calibration was performed through spectra of comparison lamps obtained with the same configuration as the science observations. Atmospheric extinction correction was based on tabulated extinction coefficients for each telescope site. Flux calibration was performed using spectrophotometric standard stars observed in the same night with the same set-up of the SN. Absolute flux calibration was then checked through comparison with the photometry. This analysis was done by integrating the spectral flux transmitted by standard *BVRI* filters. When necessary, a small multiplicative factor was applied. The resulting calibration error is ± 0.1 mag. The spectral resolutions reported in Table 7 were estimated from the FWHM of the night-sky lines. We finally used the spectra of the standard stars to remove (or reduce) the telluric features in the SN spectra. The regions of the strongest atmospheric absorptions are marked in Fig. 9. Spectra of similar quality obtained in the same night with the same telescope were combined to increase the S/N.

The spectrum of November 8 (9.2 d) revealed some problems in the flux calibration of the blue side. The spectral continuum was forced to follow the SED derived with a fourth-order polynomial fit to the photometry obtained in the same night. This spectrum will not be used to estimate the continuum temperature in Section 3.4.

3.2 Spectra analysis

Fig. 9 shows the entire evolution of SN 2007od from the first spectrum (near the *R*-band maximum) to about 1 year later. The evolution is very well sampled in the photospheric phase. As for the photometry, the transition from photospheric to nebular stages was not observed because the SN was behind the Sun. Line identification relies on qualitative arguments based on the presence of lines of the same ions at consistent velocity and by comparison with template spectra of other SNe IIP, e.g. 2005cs (Pastorello et al. 2006), 2004et (Maguire et al. 2010) and 1999em (Baron et al. 2000; Elmhamdi et al. 2003b; Pastorello 2003). For most of them, detailed line identification was carried out also with spectral modelling.

The first spectra (5–13 d) are characterized by a blue continuum, yet cooler than those of SNe 1999em and 2005cs (cf. Fig. 11). The most prominent features (Fig. 10, top) are the H Balmer lines and He I λ5876, all with a normal P-Cygni profile except Hα which shows a weak absorption component and a boxy emission. This profile, which resembles a detached atmosphere profile (Jeffery & Branch 1990), might be the signature of a weak interaction with a low-density circumstellar matter (CSM) (e.g. SN 1999em; Pooley et al. 2002).

Two absorption features are worth mentioning: one is prominent on the blue side of Hβ at about 4440 Å [marked as high-velocity (HV) Hβ in Fig. 10, top] and the other, much fainter, on the blue side of Hα, at about 6250 Å in the first spectrum (marked as Si II in Fig. 10, top). These lines were noted before in the spectra of SNe IIP. In the case of SN 2005cs (Pastorello et al. 2006), the feature near 4440 Å was identified as N II λ4623, supported by the presence of another N II line at about 5580 Å. The latter line is not seen in the spectra of SN 2007od at the expected position. Baron et al. (2000) discussed such lines in an early spectrum of SN 1999em. While the parametrized SYNOW code suggested that the 4400-Å feature was consistent with N II, the non-LTE code PHOENIX rejected this identification because of the absence of the feature around 5580 Å. Instead, the positions of both features were consistent with being Balmer lines produced in a HV layer. Such combined identification does not seem plausible in the case of SN 2007od, because the expansion velocity of the HV Hβ line is much faster than that of the putative HV Hα (25 000 versus 15 000 km s^{-1}).

In our first set of spectra (5–13 d), another absorption line is visible around 3980 Å, between Hγ and the H&K doublet of Ca II. This feature (marked as HV Hγ in Fig. 10, top) has the same velocity of the mentioned HV Hβ ($\sim$25 000 km s^{-1}) and might therefore be produced in the same layer. Up to phase $\sim$13 d, the trend of these lines is the same. From day 17 the HV Hγ disappears, likely hidden by the increasing strength of metal lines such as Fe II and Ti II. We

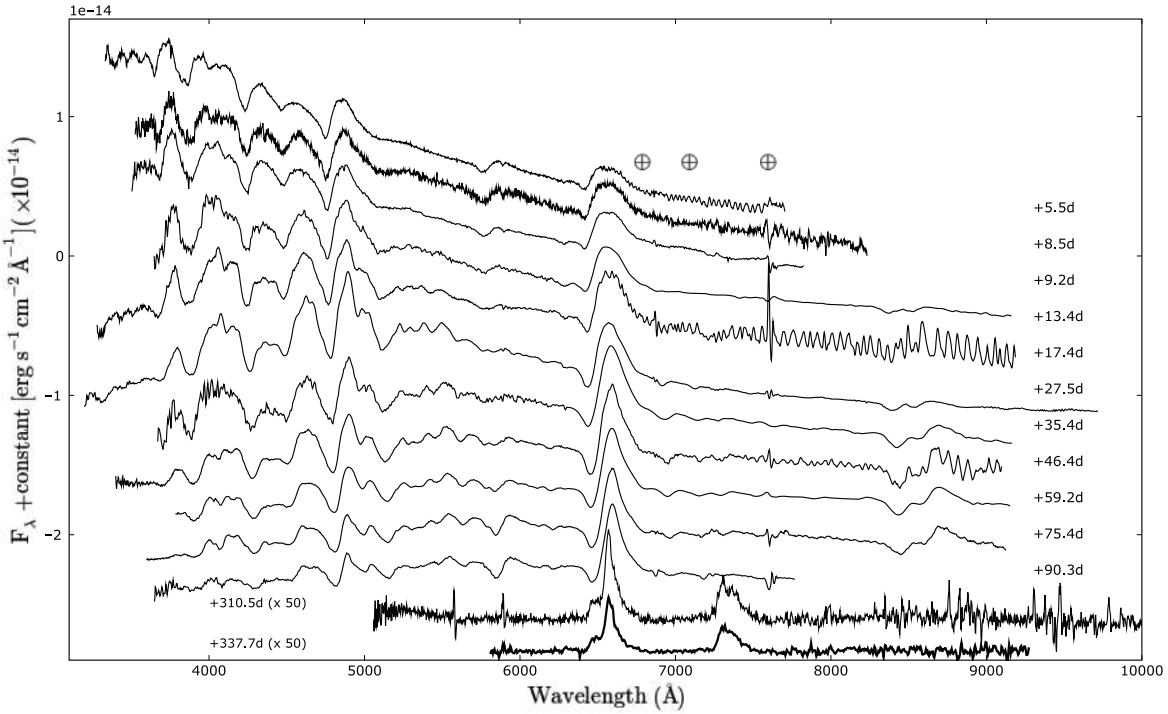

Figure 9. The overall spectral evolution of SN 2007od. Wavelengths are in the observer's rest frame. The phase reported for each spectrum is relative to the explosion date (JD 245 4404). The ⊕ symbols mark the positions of the strongest telluric absorptions. The ordinate refers to the top spectrum; the other spectra are shifted downwards with respect to the previous one by 2×10^{-15} (second spectrum), 4.3×10^{-15} (third) and 2.2×10^{-15} erg s^{-1} cm^{-2} Å^{-1}(others).

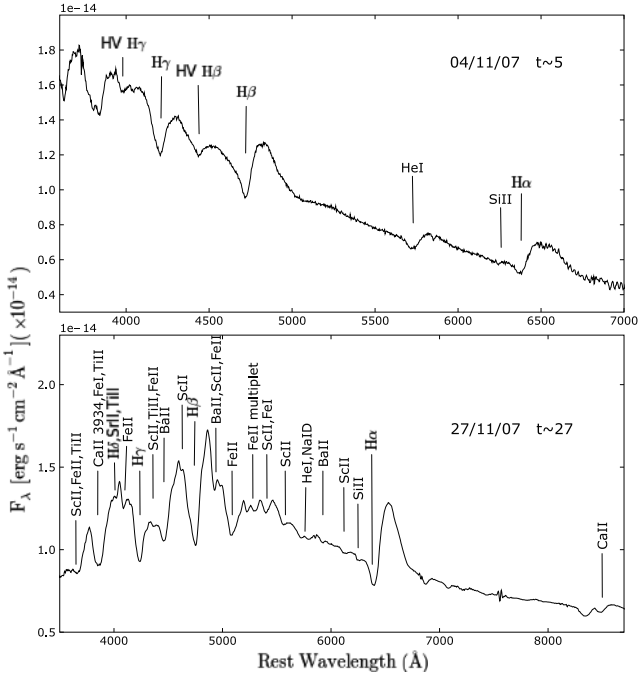

Figure 10. Top: optical spectrum of SN 2007od, obtained 5 days past explosion (JD 245 4404). Bottom: optical spectrum of SN 2007od, 27 days past explosion. Both spectra have been corrected for absorption in our galaxy and corrected by redshift. The most prominent absorptions are labelled.

suggest that these are indeed HV Balmer lines and that the HV Hα component is missing because Hα level is mostly populated collisionally, similarly to what is seen in SN IIL (Branch et al. 1981). This difference among the Balmer lines can be noted also in the early spectra of SN 1993J, which showed a more pronounced P-Cygni absorption for Hβ and Hγ than for Hα. We also mention the possibility that a contribution to the 4440-Å and the 3980-Å features is given by He I λ4471 and Hδ, respectively. However, an extensive study with SYNOW and PHOENIX on the early spectra of SN 2007od (Inserra et al., in preparation) seems to favour the identification of the two features with HV components of Hβ and Hγ.

In the early spectra of SN 2007od, H&K of Ca II and a combination of Fe I, Ti II and Sc I around 4000 Å are also identified. The line at about 6250 Å is probably Si II λ6355 as suggested by the expansion velocity, consistent with that of the other metal ions. The presence of Si II is fully blown at early times in Type Ia, but also proposed in several Type II SNe such as 2005cs (Pastorello et al. 2006), 1992H (Clocchiatti et al. 1996), 1999em (Dessart & Hillier 2005) and 1990E (Schmidt et al. 1993).

In the spectrum of November 12 (phase = 13.4 d), a faint feature appears at about 6200 Å and is probably due to Sc II (λ6300) or Fe II (λ6305). In this spectrum, there is also evidence of a feature at about 6375 Å, close to the blue edge of the Hα absorption, possibly due to Fe II λ6456. The 13.4-d spectrum, the first extending to 1 μm, shows the presence of the Ca II IR triplet ($\lambda\lambda$ 8498, 8542, 8662).

In the subsequent set of spectra (phase 17–90 d), a number of well-developed features with P-Cygni profiles appear, in addition to the persistent Balmer lines of H (Fig. 10, bottom). In the region between Hβ and Hγ, a group of lines identified as Sc II, Ti II and Fe II around 4420 Å, Ba II at λ4450 and Sc II λ4670 (on the blue side of Hβ) become more prominent than in earlier spectra. At this phase several other metal lines appear. The Fe II multiplet 42 lines ($\lambda\lambda$ 4924, 5018, 5169) are visible to the red side of Hβ along with Fe I and Sc II in the region between 5200 and 5500 Å and, starting from day 17, Sc II λ5658. Other features are identified as a blend of Ba II λ4997 and Sc II λ5031 on the red side of Hβ and Sc II λ6245. On day 27, the He I λ5876 line is weak and blended with

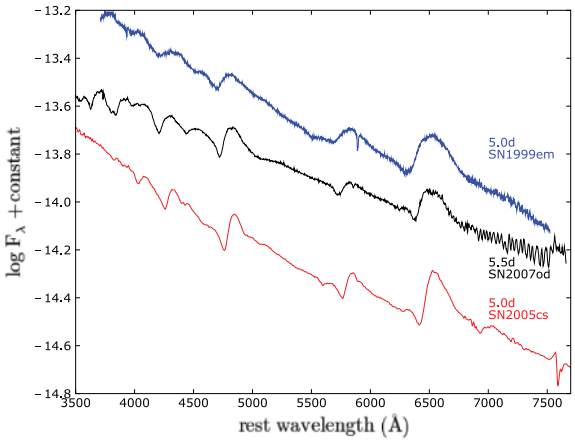

Figure 11. Comparison among spectra of SN 1999em, SN 2007od and SN 2005cs around 5 days after explosion. For references, see Section 3.3 and Table 6.

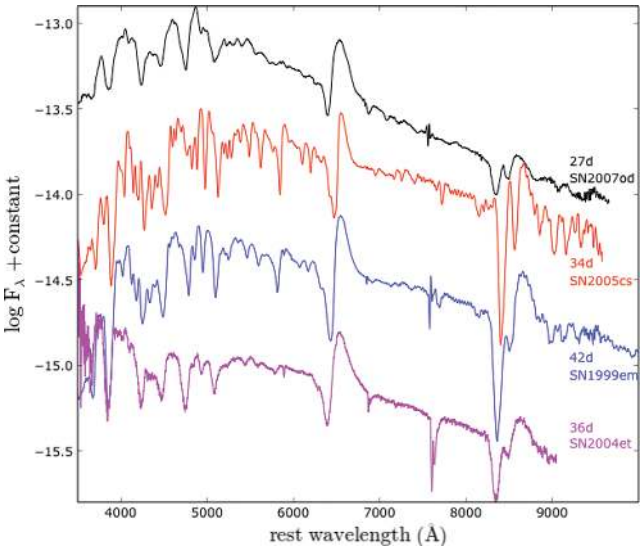

Figure 12. Comparison among spectra of SN 2004et, SN 2007od, SN 2005cs and SN 1999em during the plateau phase. For references, see Section 3.3 and Table 6.

NaID which becomes progressively stronger and replaces He I in subsequent spectra.

The presence of C I lines in spectra of Type IIP SNe was claimed in some objects, e.g. in SNe 1995V (Fassia et al. 1998) and 1999em (Pastorello 2003). In the spectra of SN 2007od at ∼75 d, a faint absorption on the red wing of Ca II IR triplet could be attributed to C I λ9061, but no other C I lines are visible to support this finding.

Two spectra are available in the nebular phase (310–338 d). In both spectra, the peaks of the Hα emission are blueshifted by the same amount (∼1500 km s^{-1}). The line shows a multicomponent structure that will be discussed in Section 4. These spectra show also forbidden emission lines of [Ca II] λλ7291, 7324, and weak evidence of [O I] λλ6300, 6364 and [Fe II] λ7155, which are common features in SNe IIP.

3.3 Comparison with other SNe

In Fig. 11 we compare the spectrum of SN 2007od at ∼5 d with two other young SNe IIP: SN 1999em (Elmhamdi et al. 2003b) and SN 2005cs (Pastorello et al. 2006). The similarity with SN 1999em was prompted by the GELATO spectral comparison tool (Harutyunyan et al. 2008), while the comparison with the faint SN 2005cs is made because of the characteristic features on the blue side of Hβ and Si II lines. All spectra show relatively blue continua and display H Balmer lines and He I 5786 Å. The spectrum of SN 2007od shows a boxy profile of Hα which suggests an ejecta–CSM interaction scenario, but no radio or X-ray observations at early phases are available to confirm such a hypothesis.

The feature at about 4440 Å, discussed in Section 3.2, is possibly detected in SN 2005cs, but not in SN 1999em. A weak line around 5600 Å, observed only in SN 2005cs (cf. Pastorello et al. 2006) and (possibly) in SN 1999em, and tentatively identified as N II, is not visible in SN 2007od.

In Fig. 12 a few spectra of Type IIP SNe during the plateau phase are compared. SN 2004et (Maguire et al. 2010) was added here because of the similarity in the bolometric light curve at early times (Fig. 8). The spectrum of SN 2007od seems to have shallower absorption components than other SNe at the same phase, probably because of temperature difference. Alternatively, this effect may be due to circumstellar interaction throughout SN 1999em toplighting effect (Branch et al. 2000). In such scenario, the fast ejecta catch and sweep up the much slower CSM from the wind of the SN progenitor (or its binary companion) and produces a continuum emission above the photosphere. The global effect is to increase the total luminosity decreasing the contrast of spectral lines. It is also possible that the reverse shock decelerates the gas and produces low photospheric velocities. The lines close to the blue edge of Hα at about 6300 Å are visible also in the spectrum of SN 2005cs and in SN 1999em but not in SN 2004et (Maguire et al. 2010).

The last comparison (Fig. 13) is made for the nebular phase with SN 1987A (Suntzeff & Bouchet 1990), SN 2005cs (Pastorello et al. 2009), SN 1999em (Elmhamdi et al. 2003b) and the luminous SN 1992H (Clocchiatti et al. 1996). The Hα profile of SN 2007od differs from those of the other SNe. The central peak is blueshifted and there is a boxy shoulder on the blue side (see Section 4). Also [Ca II] is blueshifted and shows an asymmetric profile. Instead, [O I] λλ 6300, 6363 doublet, [Fe II] at 7000 Å and NaID are barely detectable, preventing a detailed analysis of the line profiles.

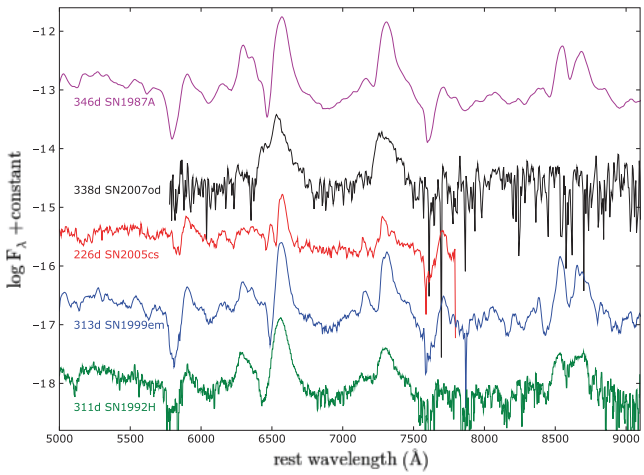

Figure 13. Comparison among spectra of SN 1987A, SN 2007od, SN 2005cs, SN 1999em and SN 1992H during the nebular phase. For references, see Section 3.3 and Table 6.

Table 8. Observed blackbody temperatures and expansion velocities of SN 2007od.

JD +240 0000	Phase[a] (d)	T (K)	v(Hα) (km s^{-1})	v(Hβ) (km s^{-1})	v(He I) (km s^{-1})	v(Fe II) (km s^{-1})	v(Sc II) (km s^{-1})
54409.5	5.5	11830 ± 350	8822 ± 104	8764 ± 164	7658 ± 122		
54412.5	8.5	9591 ± 350	8639 ± 62	8455 ± 140	7454 ± 150		
54413.2	9.2	10429 ± 350	8626 ± 60	8270 ± 140	7301 ± 100		
54417.4	13.4	9620 ± 350	8457 ± 82	8023 ± 150	7199 ± 105	5745 ± 132	5400 ± 200
54421.4	17.4	8305 ± 350	7794 ± 66	7610 ± 114	6382 ± 137	5270 ± 280	5100 ± 200
54431.5	27.5	8328 ± 350	7771 ± 75	6912 ± 130		4869 ± 200	4770 ± 110
54439.4	35.4	7123 ± 350	7565 ± 75	6425 ± 400		4515 ± 110	4161 ± 250
54450.4	46.4	5755 ± 350	6857 ± 75	5863 ± 133		3946 ± 120	3880 ± 200
54463.2	59.2	5470 ± 350	6788 ± 75	5493 ± 128		3250 ± 116	3450 ± 300
54479.4	75.4	5450 ± 350	6468 ± 95	5024 ± 100		3001 ± 120	3130 ± 200
54494.3	90.3	4429 ± 350	6308 ± 101	4777 ± 102		2736 ± 110	2670 ± 100

[a]With respect to the explosion epoch (JD 245 4404).

3.4 Expansion velocity and temperatures

The expansion velocities of Hα, Hβ, He I 5876 Å, Fe II 5169 Å and Sc II 6246 Å, derived from fits to the absorption minima, are reported in Table 8 and plotted in Fig. 14 (top panel). Error estimates are derived from the scatter of several independent measurements. The velocities of Hα are comparable with those of Hβ during the first 20 days, and progressively higher afterwards. During the 20 days in which the He I line remains visible, the velocity is about 1000 km s^{-1} smaller than that of Hα. Fe II velocity, which is a good indicator for the photospheric velocity because of the small optical depth, is lower than that of H and He I, and decreases below 3000 km s^{-1} in about three months. Sc II is also a good indicator of the photospheric velocity and its velocity is very close to that of Fe II, supporting the identifications of both ions.

In Fig. 14 (middle), we compare the Hα velocity evolution of SN 2007od with those of our comparison sample of Type IIP. In the first months, the Hα velocity of SN 2007od is comparable to those of SN 1999em, SN 2004et, SN 1992H, and higher than that of SN 2005cs, which is known to have slow photospheric expansion. As a major difference from other objects the velocity decrement is always rather constant, even in early phases. The early velocity of SN 2007od, lower than those of the other SNe of our sample, might be attributed to early-phase interaction with a low-density, thin CSM (cf. Section 3.3).

The early spectra of SN 2007od are fairly blue, suggesting moderately hot blackbody temperatures ($T_{bb} = 1.1 \times 10^4$ K). In Fig. 14 (bottom), the evolution of the temperature derived from the blackbody fits to the spectral continuum is shown and compared with those of the reference sample. The temperature evolution of SN 2007od is rather normal, although its temperature during the very first days past explosion never reached 12 000 K. About 40 days after explosion the temperature becomes constant, in analogy to what observed in SNe 2004et, 1999em and 1992H. This phase corresponds to the beginning of the H envelope recombination.

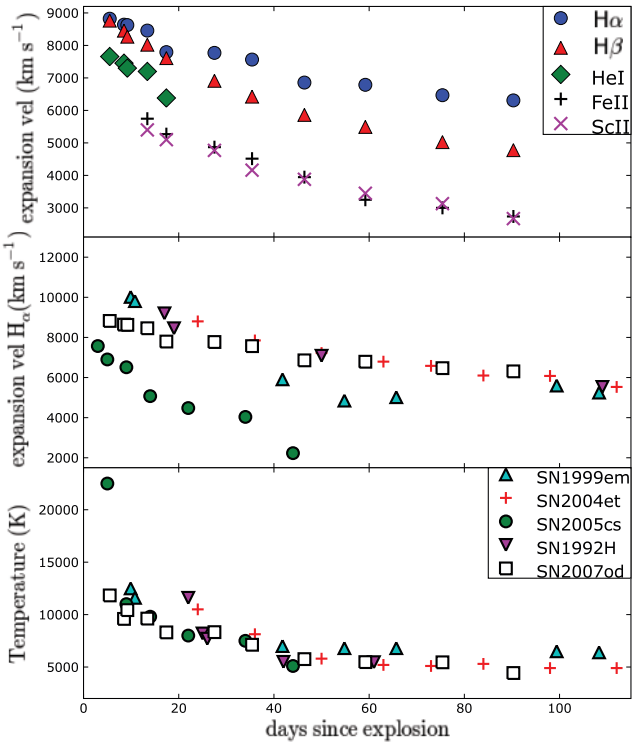

Figure 14. Top: expansion velocity of Hα, Hβ, He I λ5876, Fe II λ5169 and Sc II λ6246 as measured from the minima of the P-Cygni profiles. Middle: comparison of the Hα velocity of SN 2007od with those of other SNe II. Bottom: evolution of the continuum temperatures T_{bb} for the same SN sample.

4 DUST FORMATION AND CSM INTERACTION

Already 40 years ago it was suggested that SNe could be an important source of dust in the interstellar medium (Cernuschi, Marsicano & Codina 1967; Hoyle & Wickramasinghe 1970). Recent studies on the origin of dust (Todini & Ferrara 2001; Nozawa et al. 2003; Dwek, Galliano & Jones 2007) have supported this view, calling for core-collapse SNe (CCSNe) as significant sources of dust in the Universe. In fact, a number of objects have shown clear evidence of dust formation, e.g. Type IIn SNe 1998S (Gerardy et al. 2000; Pozzo et al. 2004), 1995N (Gerardy et al. 2002) and 2005ip (Fox et al. 2009; Smith et al. 2009); Type IIP SNe 1999em (Elmhamdi et al. 2003b), 2004et (Kotak et al. 2009; Maguire et al. 2010), 2004dj (Kotak et al. 2005; Meikle et al. 2011; Szalai et al. 2011) and 2007it (Andrews et al. 2011); Type IIb SN 1993J (Gerardy et al. 2002), the peculiar SN 1987A (Lucy et al. 1991; Arnett 1996), SN 2006jc (Mattila et al. 2008; Nozawa et al. 2008; Smith, Foley & Filippenko 2008; Sakon et al. 2009) and SN 2008S (Botticella et al. 2009). Though these data support the scenario of CCSNe being important dust producers, the amount of dust (0.1–1.0 M$_\odot$; Dwek et al. 2007; Meikle et al. 2007) required to explain the dust at high redshift is

a few orders of magnitude larger than that measured in individual local CCSNe.

There are manifold observational signatures of the formation of dust in SN ejecta. Examples are the dimming of the red wings of line profiles due to the attenuation of the emission originating in the receding layers and the steepening of the optical light curves. These effects were observed in SN 1987A (Lucy et al. 1991; Arnett 1996), SN 1998S (Pozzo et al. 2004), SN 1999em (Elmhamdi et al. 2003b) and SN 2004et (Maguire et al. 2010). Additional evidence is a strong IR excess observed in a few objects at late times, e.g. SNe 1998S and 2004et, but also, though very rarely, at early times, as in SN 2006jc. We stress that for the comprehension of the physical processes occurring in the aftermath of the explosions, it is important to distinguish between IR thermal emission from newly formed dust within the SN ejecta and IR echoes of the maximum-light emission by pre-existing, CSM.

A distinguishing precursor of dust formation is the detection of rotation–vibration molecular lines of CO, which are powerful coolants. Indeed CO was observed in several SNe, e.g. SNe 1995ad (Spyromilio & Leibundgut 1996), 1998dl and 1999em (Spyromilio, Leibundgut & Gilmozzi 2001), 2002hh (Pozzo et al. 2006), 2004dj (Kotak et al. 2005) and 2004et (Maguire et al. 2010; Kotak et al. 2009), in which also dust formation in the ejecta was detected. The presence of CO molecular lines seems, therefore, a necessary condition for dust condensation in the ejecta, as reported by Pozzo et al. (2004).

Another important issue is the site of dust formation in SNe. Indeed, dust in CCSNe has been detected (i) deep within the ejecta, e.g. in SNe 1999em and 1987A, or (ii) in a cool dense shell (CDS) created by the SN ejecta–CSM interaction, e.g. in SNe 1998S, 2004dj and 2004et. The scenarios are not exclusive and evidence of both phenomena was found, as shown in Kotak et al. (2009). Unfortunately, the paucity of MIR late-time observations makes the determination of the site of dust formation very difficult.

The signature of dust formation in SN 2007od is provided by the blueshift ($\sim$1500 km s^{-1}) of the peak of Hα, and by the corresponding attenuation of the red wing, which is seen in late-time spectra (see the panels of Fig. 15). On the other hand, the decay rates of the optical light curve between 208 and 434 d [including also data by Andrews et al. (2010), cf. Table 10] are in close agreement with the decay of ^{56}Co, suggesting that the dust formed during the period of unobservability (2008 February to May), i.e. before the late-time SN recovery (cf. Section 2.4). Indeed, Andrews et al. (2010) show that the optical and IR SED of SN 2007od at about 300 d can be fitted by the sum of a blackbody originating in the SN ejecta plus a cooler blackbody emission at 580 K due to dust.

In addition to the Hα skewed central peak, the line profile (Fig. 15) shows also the presence of structures. A boxy blue shoulder extends to about –8000 km s^{-1} (cf. Table 9), then drops rapidly to zero. This is reminiscent of the boxy profiles of late-time interacting SNe II SNe 1979C, 1980K (Fesen et al. 1999, and references therein), 1986E (Cappellaro, Danziger & Turatto 1995) which have been interpreted as evidence of interaction of the SN ejecta with a spherical shell of CSM (Chevalier 1982; Chevalier & Fransson 1994). We note that, unlike other SNe, in SN 2007od a red, flat shoulder is not visible, possibly because it is attenuated by dust intervening along the line of sight.

A hint of a narrow, unresolved emission at the Hα rest wavelength, more evident in the Gemini spectra by Andrews et al. (2010), is visible also in our latest spectrum. The peak of the [Ca II] $\lambda\lambda$ 7292, 7324 emission is also blue-skewed with attenuation of the red wing in analogy to Hα [panels (d) and (e) of Fig. 15]. Instead, [Ca II] does not show the blue shoulder indicating that the interaction does not affect the metal-enriched ejecta, as noted in Andrews et al. (2010).

Andrews et al. (2010) noted analogies between the Hα profiles of SN 2007od and SN 1998S, and tried to explain the Hα profile between 8 and 20 months as the combination of different phenomena: the interaction of the ejecta with a CSM torus and a blob of CSM out of the plane of the torus, plus the possible presence of a light echo. Each process corresponds to specific components of the line profile (cf. their fig. 4): two components at about $\pm$1500 km s^{-1}

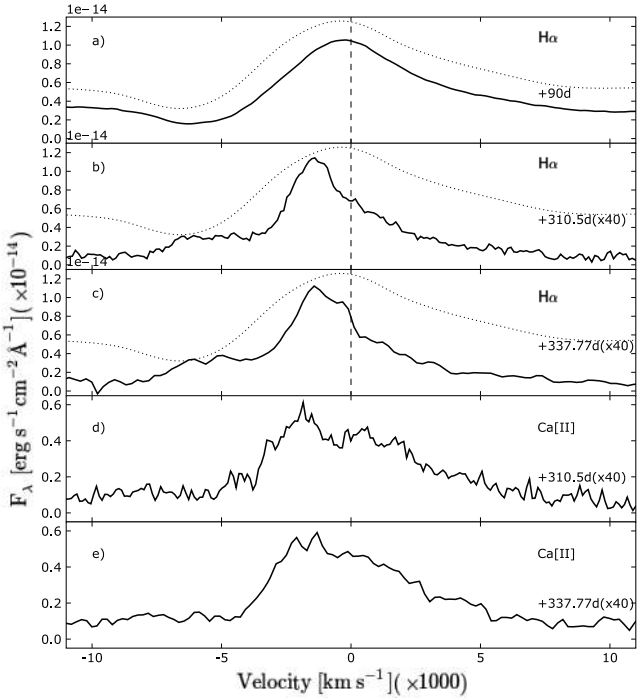

Figure 15. Zoom in the Hα region of the SN 2007od spectra at 90 d (panel a), 310 d (b) and 337 d (c). The dotted line is the photospheric spectrum on day 60 used as a comparison. Panels (d) and (e) show the [Ca II] profiles at late epochs. The abscissa is in expansion velocity coordinates with respect to the rest-frame positions of Hα and to the average position of the [Ca II] doublet. Phases relative to the explosion (JD 245 4404) are indicated on the right.

Table 9. Evolution of the Hα line profile.

Phase[a] (d)	Velocity[b] (km s^{-1})					Flux[c]
	Blue edge	Central Peak Position	FWHM	HWHM[d]	Red edge	
60		−301				
75		−319				
90		−240				
226[e]	−8270	−1325	4110	2100	7770	51.20
303[e]	−8000	−1500	2790	2010	7860	22.50
310	−8100	−1508	2815	2230	7700	22.21
337	−8090	−1568	2623	2280	7680	12.43
342[e]	−8180	−1508	2615	2200	7900	14.30
452[e]	−8100	−1100	2970	2600	7850	5.28
666/692[e]	−7400					

[a]With respect to the explosion epoch (JD 245 4404). [b]With respect to the Hα rest-frame wavelength. [c]10^{-16} erg s^{-1} cm^{-2}. [d]HWHM of the blue, unabsorbed wing computed with respect to the rest-frame wavelength. [e]Spectra from Andrews et al. (2010), flux calibrated with broad-band photometry.

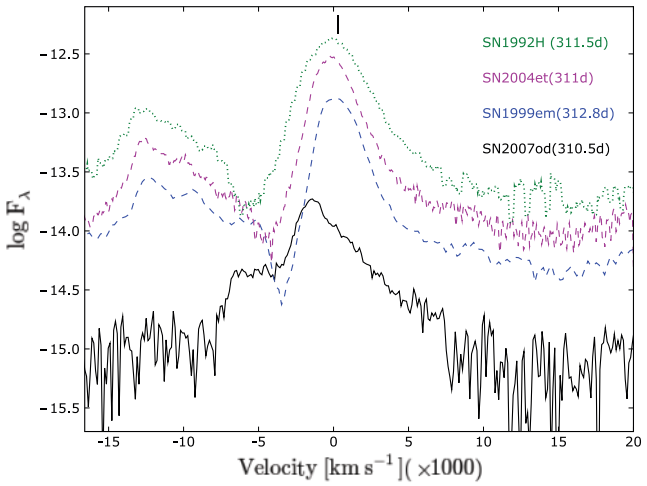

Figure 16. Comparison of the Hα profile of SN 2007od during the nebular phase with those of SNe 1992H, 1999em and 2004et. The spectra of all SNe were reported to the same distance of SN 2007od. The position of the Hα rest wavelength is marked with a vertical dash.

that arise in the radiative forward shock of the ejecta interacting with the torus which should be highly inclined to produce the low observed projected velocities; a slightly broader component at about $-5000\,\mathrm{km\,s^{-1}}$ due to the ejecta–blob interaction with a larger velocity component along the line of sight; a residual ejecta component similar to that observed on day 50, required to explain the broad red wing of the line; and a light echo that became dominant about 2 year after explosion. The blueshifted component at $-1500\,\mathrm{km\,s^{-1}}$ appears stronger than that at $+1500\,\mathrm{km\,s^{-1}}$. This asymmetry was attributed to strong extinction suffered by the receding component due to dust formed in the CDS. The weakness of this scenario is in the geometry of the torus. As mentioned above, the torus is required to have an inclination of the order of 80° (for H expansion velocity of the order of $10\,000\,\mathrm{km\,s^{-1}}$) to explain the small projected velocities. Even for a thick torus, it is difficult to reconcile the required high inclination with the strong extinction suffered by the red component. For the same ejecta velocity, the inclination of the blob along the line of sight is about 60°, i.e. it is not orthogonal to the torus.

Useful information on the phenomena taking place in SN 2007od at late times come from the comparison of the late Hα profile with those of other SNe IIP. In Fig. 16, all spectra were corrected for absorption and rescaled to the distance of SN 2007od. The line flux of SN 2007od is significantly smaller than those of other SNe. The blue, (likely) unabsorbed wing of the central/core Hα emission of SN 2007od roughly coincides in wavelength with the corresponding blue wings of other non-interacting SNe II at similar phases (we stress that SN 1999em at this epoch does not show sign of interaction). In particular, the HWHM(Hα) $\sim 2000\,\mathrm{km\,s^{-1}}$ (Table 9) of the blue side is compatible with the FWHM(Hα)$\sim$4000 km s^{-1} of the emission of SN 1992H at 311 days after explosion, a SN that has a similar kinematics to SN 2007od (cf. Fig. 14). Also the terminal velocities of Hα seem very similar, since the edge of the blue shoulder of SN 2007od extends out to $8000\,\mathrm{km\,s^{-1}}$, a velocity comparable to the bluest wing of the residual P-Cygni absorption of SN 1992H. The flux of the blue wing of the central emission (at about 6500 Å), likely less absorbed, coincides with those of other SNe II, e.g. SN 1999em. On the contrary, the flux at the rest wavelength is significantly depressed, and even more is the red wing, indicating the presence of dust within the ejecta. The resulting profile is skewed. The comparison, therefore, seems to point towards a common origin of the line cores extending between 6450 and 6650 Å as arising from the spherical expanding ejecta.

Evidence of dust in the ejecta was also seen in SN 1987A and SN 1999em. In the case of SN 1987A, the dust formed in an inner core at $v \sim 1800\,\mathrm{km\,s^{-1}}$ with optical depth $\tau \leq 1$ at a much later epoch $t \sim 526$ d (Lucy et al. 1989) than in SN 2007od. Also in SN 1999em the dust formed late ($t \sim 500$ d) when no sign of interaction was present. Here the dust location, within an inner region at $v \sim 800\,\mathrm{km\,s^{-1}}$ with $\tau \geq 10$, was derived from a careful analysis of the profile of the [O I] λλ6300, 6363 doublet (Elmhamdi et al. 2003b). As already mentioned, the [O I] doublet is barely visible in the late spectra of SN 2007od, and the analysis relies on the line profile of Hα which arises mainly from the outer ejecta.

As for the CSM/ejecta geometry proposed by Andrews et al. (2010) to explain the Hα profile, the formation of dust deep within the ejecta of SN 2007od is also not devoid of problems. In fact, at the early epoch of occurrence ($t \leq 226$ d), the SN ejecta are expected to be too warm for dust condensation (Kozasa, Hasegawa & Nomoto 1991), while the presence of interaction at this phase justifies the dust formation in an outer CDS. It is possible that SN 2007od was intrinsically less energetic than average CCSNe, similar to low-luminosity SNe like 1997D and 2005cs, and that the temperature at about 200 days was already low enough to allow dust condensation in some regions of the SN ejecta.

Observations show first evidence of interaction already on day 226. At this epoch the ejecta reached the material expelled by the progenitor in mass-loss episodes at short times before explosion. The interaction produces forward and reverse shocks (Chevalier 1982). In general, between the two shocks, the gas undergoes thermal instability and cooling, thus creating a CDS in which subsequently dust can form. The formation of a CDS can take place behind the forward shock primarily in the CSM, as invoked in the case of SN 2006jc by Mattila et al. (2008), or behind the reverse shock as in SN 1998S (Pozzo et al. 2004). With a standard mass-loss rate, the CDS forms behind the reverse shock, i.e. in the ejecta that are denser and chemically richer, hence more prone to dust formation (Pozzo et al. 2004). The presence of dense clumps in the CSM, which eventually are overcome by the fast SN ejecta, may allow the formation of a CDS (and dust) also in regions that eventually are deeply embedded in the ejecta.

We believe that the observed late-time line profiles at about 300 days can be explained schematically with (1) a relatively broad skewed emission from SN ejecta (FWHM $\sim 2800\,\mathrm{km\,s^{-1}}$) typical of SNe II at corresponding epochs, significantly absorbed by dust formed *within the ejecta, possibly in clumps*; (2) a distorted boxy profile with HV (up to $8000\,\mathrm{km\,s^{-1}}$), evidence of the interaction of the H-rich ejecta with a *spherical* outer CSM, with the red shoulder depressed due to dust absorption. The presence of late-time interaction is supported by the re-brightening of optical light curves by day ∼653, as shown by Andrews et al. (2010); (3) an unresolved emission which forms in the unshocked CSM (cf. Andrews et al. 2010).

A plausible scenario to explain the observed structure of Hα could be similar to that proposed for SN 1988Z (Chugai & Danziger 1994). The ejecta collide with a two-component wind: a spherically symmetric substrate composed of a relatively rarefied gas and very dense clumps (cf. Fig. 17). Such structure allows the formation of the boxy profile due to the interaction between the fast expanding ejecta and the CSM and, at the same time, the early formation of dust deep in the ejecta in the CDS of the inner clumps. The dust inside the ejecta progressively screens the radiation arising from

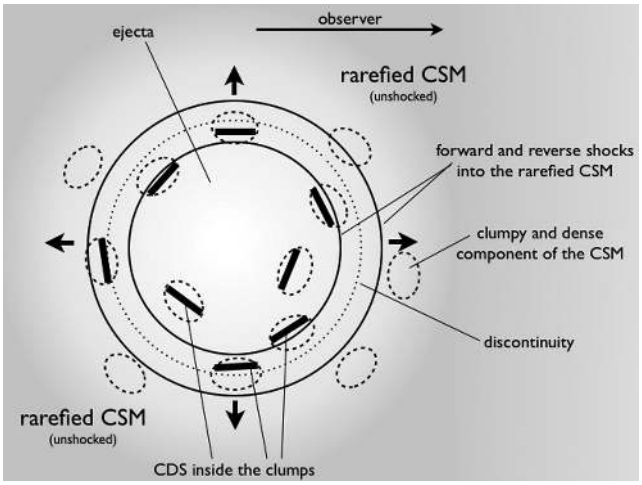

Figure 17. Schematic illustration of the geometry of the newly formed dust in SN 2007od. The CDS arises both inside the dense clumps and between the reverse shock and the discontinuity of the rarefied component of the CSM.

the receding layers and skews both the central profile from the unperturbed ejecta and the boxy profile from the interaction. Indeed the profile of Hα suggests the presence of dust also in the inner ejecta since dust formation in the outer CDS dims both the blue and red wings in the same way, and the red shoulder would appear boxy and not tilted (Fig. 15).

The analysis of the IR SED performed by Andrews et al. (2010) shows a strong IR excess attributable to warm dust, consistent with an amorphous carbon dominated model with 75 per cent amorphous carbon and 25 per cent silicate. The radiative transfer models used by Andrews et al. (2010) suggest up to $4.2 \times 10^{-4}\,M_{\odot}$ dust, mainly composed of amorphous carbon grains formed in a CDS.

The flat blue shoulder of Hα is barely visible in the spectrum taken on day 226 but is very well formed on day ∼337 when the emission extends out to ∼8200 km s^{-1}, and remains well defined until day 680 (Andrews et al. 2010). Assuming that the CSM is due to the mass loss of material travelling at 10 km s^{-1}, this indicates the presence of CSM in a range of distances of about 1300–1950 au and that the progenitor experienced enhanced mass loss 500–1000 yr before the explosion.

5 DISCUSSION

In the previous sections, we presented new data of the Type II SN 2007od in UGC 12846, including for the first time photometric and spectroscopic observations of the early epochs after the explosion.

Analysis of the multicolour and bolometric light curves indicates that at early times SN 2007od was a luminous SN IIP like SNe 1992H and 1992am. The absolute magnitude at maximum, $M_V = -18.0$, the bolometric luminosity $L_{\rm bol} = 6.0 \times 10^{42}$ erg s^{-1} (see Table 10), and the relatively short plateaus in V and R suggest an envelope mass smaller than that of standard plateau events.

SN 2007od shows several interesting properties. At early epochs ($t < 15$ d), $T_{\rm bb}$ and $v_{\rm exp}$ are lower than in other bright SNe II, e.g. SN 1992H and SN 2004et. In the same period, the Hα emission component is squared, and there is evidence for HV features in Hβ and Hγ. These properties, together with bright luminosity and shallow absorption features, point towards early interaction of the ejecta with a low-density CSM (cf. Moriya et al. 2010). The absence of X-ray or radio detection is not against this scenario, because the distance to SN 2007od is 26 Mpc, much larger than that of SN 1999em (7.5–7.8 Mpc). If for SN 2007od we assume the same radio and X-ray luminosity of SN 1999em, the observed flux should be below the threshold of the observation. Indeed the X-ray flux of SN 1999em was close to the limit (about 10^{-14} erg cm^{-2} s^{-1}) as well as the radio flux reported in Pooley et al. (2002). If SN 2007d had the same emission of SN 1999em, the expected X-ray flux would be about 10^{-15} erg cm^{-2} s^{-1}, much lower than the 3σ upper limit by Immler & Brown (2007). Moreover, HV features in optical spectra were proposed by Chugai, Chevalier & Utrobin (2007), as clues of interaction and detected in SN 1999em and SN 2004dj. We claim that this is the case also for SN 2007od. A rough estimate of the CSM mass in close proximity to the progenitor can be derived starting by SYNOW parametrization of the early spectra. Through the optical depth of HV lines ($\tau = 0.8$) we can gain the H density in the transition. Thanks to the Saha equation in local thermodynamic equilibrium (LTE) approximation, it is possible to obtain the ratio between HI ($n_{\rm H\,I} = 1.7 \times 10^{-30}$ to 1.4×10^{-31} based on different assumptions) and the total H density. This ratio is roughly related to the mass of the CSM. In our case we estimated a CSM mass of the order of $\sim 10^{-3}$–$10^{-4}\,M_{\odot}$. This value is in agreement with the velocities of the HV lines reported in Section 3.2, in fact a greater amount of CSM would not allow reaching such velocities.

The light curves show a drop of ∼6 mag from the plateau to the tail. The tail is therefore relatively faint, corresponding to a ^{56}Ni mass $M(^{56}\mathrm{Ni}) \sim 3 \times 10^{-3}\,M_{\odot}$, unusually small for SNe IIP that are luminous at maximum and are comparable to those estimated in faint SNe IIP such as SN 2005cs. In Section 4 we show spectroscopic evidence of dust formation at late times and therefore that the derived amount of ^{56}Ni should be considered as a lower limit. A more solid estimate, based on the bolometric flux including the MIR late-time emission by Andrews et al. (2010), is $M(^{56}\mathrm{Ni}) \sim 2 \times 10^{-2}\,M_{\odot}$, thus indicating that about 90 per cent of the optical+NIR emission is reprocessed by dust.

Dust formation occurs within day 226 after the explosion, quite early in comparison to other CCSNe, e.g. SN 1987A, SN 1999em and SN 2004et. To our knowledge, SN 2007od is the Type IIP SN showing the earliest dust formation. Late-time optical spectroscopy shows also clear signs of strong ejecta–CSM interaction. Indeed, the complex Hα profile can be interpreted as the combination of a typical ejecta emission, ejecta–CSM interaction and the presence of dust in clumps. However, the combined effect of interaction and dust does not affect the decline rate that is similar to that of ^{56}Co decay from 208 to ∼434 d past explosion (Fig. 6). CSM–ejecta interaction makes a minor contribution to the bolometric luminosity and only affects line profiles. A flattening of the light curve might be present after day 600 as shown in Andrews et al. (2010), either because of increased interaction or a light echo, but the data are too inhomogeneous for a strong statement in this sense.

Because of the location in the outskirts of the parent galaxy, the metallicity at the position of SN 2007od could not be determined from our spectra nor were we able to find spectra of the host galaxy in the main public archives. UGC 12846 is classified as Magellanic Spiral (Sm:) of low surface brightness (LSB), as confirmed by our Fig. 1 (left) in which the host galaxy is barely visible. LSB galaxies are objects with peak surface brightness $\mu^B_{\rm peak} \geq 22.5$–23 mag arcsec^{-2} having generally low metallicity [$Z < (1/3)Z_{\odot}$ (McGaugh 1994); $0.1 < Z(\mathrm{LSB})/Z_{\odot} < 0.5$, with no radial dependence (de Blok & van der Hulst 1998)]. Smoker, Axon & Davies (1999) and Smoker et al. (2000) for UGC 12846 report a central surface brightness $\mu^B_{\rm peak} \sim 22.65$ decreasing to $\mu > 26$ mag arcsec^{-2} at position of the SN. Using $M_B = -16.79$ (Smoker et al. 1999) and the

Table 10. Main data of SN 2007od.

Position (2000.0)		$23^h55^m48^s.68$	$+18°24^m54^s.8$
Parent galaxy		UGC 12846, Sm:	
Offset w.r.t. nucleus		38″E	31″S
Adopted distance modulus		$\mu = 32.05 \pm 0.15$	
SN heliocentric velocity		$1734 \pm 3\,\mathrm{km\,s^{-1}}$	
Adopted reddening		$E_g(B-V) = 0.038$	$E_{tot}(B-V) = 0.038$
	Peak time (JD 245 4000+)	Peak observed magnitude	Peak absolute magnitude
U	409 ± 2	13.490 ± 0.04	-18.7 ± 0.18
B	409 ± 2	14.464 ± 0.03	-17.8 ± 0.18
V	411 ± 2	14.144 ± 0.02	-18.0 ± 0.23
R	411 ± 2	13.945 ± 0.02	-18.1 ± 0.21
I	411 ± 2	13.821 ± 0.02	-18.2 ± 0.23
uvoir	410 ± 2	$L_{bol} = 6.0 \times 10^{42}\,\mathrm{erg\,s^{-1}}$	
Rise to *R* max	∼5 d		
Explosion day	$\sim 404 \pm 5$	∼ 2007 Oct. 30	
		Late-time decline mag(100 d)$^{-1}$	Interval (d)
V		0.94	208–434
R		1.00	208–434
I		1.08	208–434
uvoir		1.053	208–434
UBVRI		1.065	208–434
M(Ni)		$0.02\,M_\odot$	
M(ejecta)		$5–7.5\,M_\odot$	
Explosion energy		0.5×10^{51} erg	

diagram shown in McGaugh (1994), we can consider UGC 12846 as a LSB with average oxygen abundance. Therefore, the environment of SN 2007od is likely metal poor with log(O/H) ∼−4. In general, we expect that low-metallicity stars suffer little mass loss and have big He cores and massive H envelopes when they die (Heger et al. 2003). The significant presence of CSM both at early and late times, a clear evidence of mass loss, seems in disagreement with this scenario, although recently Chevalier (2008) suggested that there are mass-loss mechanisms that do not decline at lower metallicities. Alternatively, the presence of companions can explain strong mass loss by metal-poor stars.

In nebular spectra of CCSNe, the flux ratio $R = \frac{[\mathrm{Ca\,II}]\lambda\lambda 7291,7324}{[\mathrm{O\,I}]\lambda\lambda 6300,6364}$ is almost constant with time (Fransson & Chevalier 1987; 1989). This ratio, only marginally affected by differential reddening, is a useful diagnostic for the mass of the core and consequently for estimating the progenitor mass, with small ratios corresponding to higher main-sequence masses. In SN 1987A it was $R \sim 3$ (Elmhamdi et al. 2003a), for the faint SN 2005cs it was $R \sim 4.2 \pm 0.6$ (Pastorello et al. 2009), while for SNe 1992H and 1999em we computed the values $R \sim 1.61$ and 4.7, respectively. In comparison, the measured ratio $R \sim 32 \pm 5$ of SN 2007od is very high, suggesting that the progenitor mass is quite small.

A super-asymptotic giant branch (SAGB) progenitor with a strongly degenerate Ne–O core might explain these observables. As shown by Pumo et al. (2009), the most massive SAGB stars ($M \lesssim M_{mas} \sim 10–11\,M_\odot$) can indeed suffer strong episodes of mass loss while still preserving significant H envelopes ($\gtrsim 5–9\,M_\odot$) at the end of their evolution. In fact, the outcome of SNe from a SAGB progenitor can differ according to the configuration of the SAGB star at the moment of the explosion, and may range from a Type II SN (either IIP or IIL depending on the mass of the envelope) with relatively low degree of CSM interaction to a Type IIb SN having stronger interaction with the CSM, up to a stripped-envelope SN. The high value of *R* could be explained also with Fe CCSNe II in the low limit of the mass range (∼11–12 $M_\odot$); these stars might produce oxygen-poor SNe II. But these stars hardly explain the episodes of mass loss at metallicities lower than solar (Woosley, Heger & Weaver 2002). Binary companions could easily explain the episodes of mass loss, regardless of the progenitor star. We cannot exclude a priori the binary system solution.

The formation of dust plays a key role in shaping the display of SNe II. In SN 1998S, Pozzo et al. (2004) calculated a value of $\sim 10^{-3}\,M_\odot$ of dust in a CDS. Elmhamdi et al. (2003b) obtained a lower limit of $\sim 10^{-4} M_\odot$ in the ejecta of SN 1999em from the analysis of the [O I] 6300 Å evolution. For SN 1987A, Ercolano, Barlow & Sugerman (2007) reported a dust mass of $7.5 \times 10^{-4}\,M_\odot$. For SN 2004et, Kotak et al. (2009) estimated a dust mass of $M = (2–5) \times 10^{-4}\,M_\odot$ in the CDS, and through hydrodynamical considerations suggested that the mass of new dust produced either in the ejecta or in a CDS never exceeded $10^{-3}\,M_\odot$. The formation of $(1.7–4.2) \times 10^{-4} M_\odot$ of dust (Andrews et al. 2010) contributes to the unusual drop of ∼6 mag (from plateau to tail) in SN 2007od.

The dust mass estimate can change by an order of magnitude if we consider silicates or carbon grains and if we take into account the possibility of very opaque clouds (Elmhamdi et al. 2003b; Pozzo et al. 2004). Indeed, when forming in clumps most of the dust could be undetectable due to the clump opacities, and could be in much higher amounts than necessary to produce the observed blackbody emission. We note that the environment of this SN is different from other dust-forming SNe that normally explode in spiral galaxies or

in regions with solar metallicity. Indeed, the environment metallicity of SN 2007od is between solar and that of galaxies at $z \gtrsim 6$. Thus, one may speculate that larger amounts of dust are formed at high redshift because of low metallicities.

5.1 Explosion and progenitor parameters

We estimated the physical properties of the SN progenitor (namely the ejected mass, the progenitor radius and the explosion energy) by performing a simultaneous χ^2 fit of the main observables (i.e. bolometric light curve, evolution of line velocities and continuum temperature at the photosphere) against model calculations, in analogy to the procedure adopted for other SNe (e.g. SNe 1997D, 1999br, 2005cs; Zampieri et al. 2003; Zampieri 2007).

Two codes were used to produce models: a semi-analytic code (described in detail in Zampieri et al. 2003) which solves the energy balance equation for a spherically symmetric, homologously expanding envelope of constant density and a new, relativistic, radiation-hydrodynamics code [described in detail in Pumo, Zampieri & Turatto (2010) and Pumo & Zampieri (in preparation)]. The latter is able to compute the parameters of the ejecta and the emitted luminosity up to the nebular stage by solving the equations of relativistic radiation hydrodynamics in spherically symmetry for a self-gravitating fluid which interacts with radiation, taking into account the heating due to decays of radioactive isotopes synthesized in the SN explosion.

The semi-analytic code was used to perform a preparatory study in order to constrain the parameter space and, consequently, to guide the more realistic but time-consuming simulations performed with the relativistic radiation-hydrodynamics code. We note that modelling with these two codes is appropriate if the emission from the SN is dominated by the expanding ejecta. For SN 2007od, the contamination from interaction and the formation of dust may in part affect the observed properties of the SN during the first ∼20 d and from the end of the plateau afterwards. However, there is no evidence that either interaction or dust formation is important during most of the photospheric phase (∼20–90 d) and hence our hydrodynamic modelling can be safely applied to SN 2007od during this time frame. This is more than sufficient for providing a reliable estimate of the main physical parameters of the ejecta, with the exception of the Ni mass that, as already mentioned, is inferred from late-time optical and NIR observations.

The shock breakout epoch (JD = 245 4404 ± 5) and distance modulus ($\mu = 32.05 \pm 0.15$) adopted in this paper (cf. Section 2.5) are used to fix the explosion epoch and to compute the bolometric luminosity of SN 2007od for comparison with model calculations. Assuming a ^{56}Ni mass of 0.02 $M_\odot$ (see Section 2.6), the best fits of the semi-analytic and numerical models are in fair agreement and return values of total (kinetic plus thermal) energy of ∼0.5 foe, initial radius of (4–7) × 10^{13} cm and envelope mass of 5–7.5 $M_\odot$ (Fig. 18).

The best-fitting models show some difficulty in reproducing the early part of the light curve ($\lesssim$25 d) and the very end of the apparent plateau (at ∼106 d). The excess at early epochs may be caused in part by the ejecta–CSM interaction (see discussion in Section 5). As for the point at ∼106 d, the excess may be related to the final interaction stage with the H-rich CSM that occurs at the end of the recombination phase.

In Fig. 18, we show also the evolution of the photospheric velocity and temperature. The agreement between our modelling and the observational data is good apart from, once again, the early phase. The reason for this difference may be due to both interaction and the approximate initial density profile used in our simulations, which may not reproduce correctly the radial profile in the outermost HV shells of the ejecta formed after shock breakout (e.g. Utrobin 2004, Pumo & Zampieri, in preparation). For this reason, we did not include the first three measurements of the line velocity in the fit.

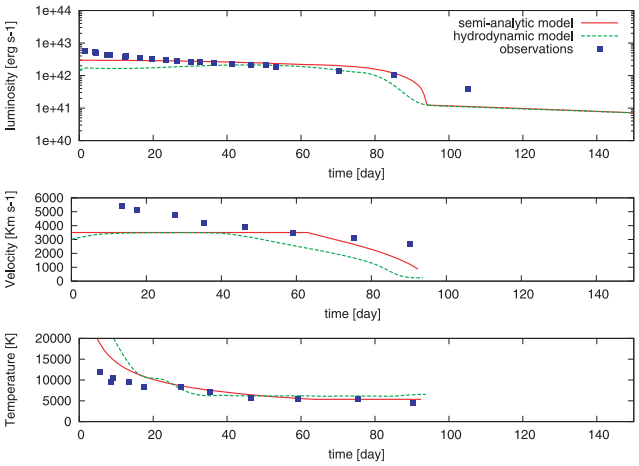

Figure 18. Comparison of the evolution of the main observables of SN 2007od with the best-fitting models computed with the semi-analytic code (total energy ∼0.5 foe, initial radius 4 × 10^{13} cm, envelope mass 5 $M_\odot$) and with the relativistic, radiation-hydrodynamics code (total energy ∼0.5 foe, initial radius 7 × 10^{13} cm, envelope mass 7.6 $M_\odot$). Top, middle and bottom panels show the bolometric light curve, the photospheric velocity and the photospheric temperature as a function of time, respectively. To estimate the photosphere velocity from observations, we used the value inferred from the Sc II lines (often considered in Type II SNe as good tracer of the photosphere velocity).

The values of the modelling reported above are consistent with the explosion and mass loss of a SAGB star with an initial (ZAMS) mass $\lesssim M_{\rm mas}$ [$M_{\rm mas} \sim 9.7$–$11.0\,M_\odot$ for the environment metallicity limits of Pumo et al. (2009), cf. Section 5, see also Pumo et al. (2009) for details]. The moderate ejecta mass and amount of ^{56}Ni, the relatively low explosion energy, the very large Ca/O ratio and the presence of C-rich dust fit reasonably well within this framework.

Some of these constraints may appear consistent with a fallback SN from a massive star. In this scenario the mass-cut is located sufficiently far out to trap part of the ^{56}Ni and intermediate mass elements (e.g. O) that fall back on to the compact object. Also the relatively low explosion energy may be related to this mechanism (Fryer 1999; Zampieri 2002). However, significant mass loss prior to explosion is not easy to reconcile with a high-mass progenitor in a low-metallicity environment (see Section 5). Problematic are also the moderate amount of ^{56}Ni estimated including MIR data, the relatively high expansion velocity and low ejecta mass, and the C-rich dust (Andrews et al. 2010), since usually these stars produce silicate-rich dust (Kotak et al. 2009, and reference therein).

6 CONCLUSIONS

In this paper we present new early- and late-time observations of SN 2007od. The SN is among the brightest Type IIP SNe known to date (peak magnitudes $M_R = -18.1$ and $M_V = -18.0$), and shows evidence of interaction with CSM both at early and late times. These observations, along with dust formation at late epochs, make this object different from common IIP events.

The light curve of SN 2007od reaches a bright, short plateau lasting ∼25 d at $M_R = -17.8$ after a short post-peak decline in which

the luminosity decreases by 0.3 mag in a few days. The early high brightness is coupled with a low-luminosity tail comparable to that of the faint SNe, e.g. SN 2005cs. The magnitude drop from the plateau to the first available point of the tail is ∼6 mag, unusually large for a SN IIP. The bolometric light curve tail roughly follows the slope expected for ^{56}Co decay into ^{56}Fe. The ^{56}Ni mass derived from the late-time *uvoir* (*UV* to *K*) luminosity is $M(\mathrm{Ni}) \sim 3 \times 10^{-3}\,\mathrm{M}_{\odot}$. Late-time (200–700 d) optical spectroscopy and MIR photometry (after 300 d; Andrews et al. 2010) show clear evidence of dust formation. The Ni mass derived including the MIR blackbody emission due to dust indicates a much larger $M(\mathrm{Ni}) \sim 2 \times 10^{-2}\,\mathrm{M}_{\odot}$.

The early spectra show the presence of Si II, a boxy Hα profile and extreme ($\sim$25 000 km s^{-1}) HV features of the Balmer lines. The material ejected at HV is compatible with a CSM mass of the order of $\sim 10^{-3}$–$10^{-4}\,\mathrm{M}_{\odot}$ located close to the exploding star. The interaction of the ejecta with a thin, moderately dense CSM might increase the luminosity of the light curves and reduce the duration of the plateau (part of the H envelope of the star is lost and the H mass that recombines is smaller). Finally, the expansion velocity and blackbody temperature are comparable to those of Type II such as SN 1992H and SN 2004et until the tail.

Late spectra show weaker [O I] than other SNe II, evidence of ejecta–CSM interaction and early dust formation. The boxy line profile of Hα was interpreted as the interaction of spherically symmetric SN ejecta expanding in a medium of low average density, but with dense clumps. A similar configuration was invoked for SN 1988Z (Chugai & Danziger 1994), and allows for the early formation of dust in a CDS inside clumps that eventually become incorporated within the SN ejecta. Radiative transfer models (Andrews et al. 2010) have provided estimates of the total dust mass up to $4.2 \times 10^{-3}\,\mathrm{M}_{\odot}$, which may represent only a lower limit due to its clumpy distribution.

Only at epochs later than 500 d, when the light curve flattens, the interaction might dominate over other sources of energy.

SN 2007od exploded in a LSB galaxy, presumably in a low-metallicity environment with $\log(\mathrm{O/H}) \sim -4$. In general, low-metallicity stars suffer less mass loss than higher metallicity counterparts, so that it appears likely that the significant mass loss probed by the interactions occurred because the progenitor was a SAGB star that still preserved H before the final explosion (Pumo et al. 2009). This is compatible with the results of our modelling of the SN observables.

SN 2007od shares many properties with both Type IIn and typical Type IIP objects. Our analysis has provided indications that (1) HV features are present also in CCSNe; (2) early ejecta–CSM interaction can be significant also for SNe IIP; (3) dust formation can occur very early in the SN evolution and affect both the photometric and the spectroscopic behaviour significantly and (4) extended sampling of the SED is essential to describe all phenomena characterizing the CCSN evolution. The properties of the 'beasts' of the CCSN zoo do not cease to be amazing.

ACKNOWLEDGMENTS

CI is grateful to professor Lucio Paternò for useful advice and suggestions in the earliest stages of his PhD course. CI is also grateful to Eddie Baron and David Branch for countless discussions and suggestions, and for hospitality at the University of Oklahoma. The authors thank J. Andrews for providing the late-time digital spectra of SN 2007od. The authors also thank J. Vinko for the useful suggestions. SB, FB, EC, MDV and MT are partially supported by the PRIN-INAF 2009 'Supernovae Variety and Nucleosynthesis Yields' and by the grant ASI-INAF I/009/10/0. MLP acknowledges the financial support by the Bonino-Pulejo Foundation. The TriGrid VL project, the '*consorzio COMETA*' and the INAF - Padua Astronomical Observatory are also acknowledged for computer facilities. We thank the support astronomers at the Telescopio Nazionale Galileo, the Copernico Telescope at Cima Ekar, the 2.2-m Telescope at Calar Alto, the Nordic Optical Telescope, the New Tecnology Telescope, the Galileo Galilei Telescope on Cima Pennar and the Hale Telescope on Palomar Observatory for performing the follow-up observations of SN 2007od. This research has made use of the NASA/IPAC Extragalactic Data base (NED) which is operated by the Jet Propulsion Laboratory, California Institute of Technology, under contract with the National Aeronautics and Space Administration. This research has made use of data obtained from the High Energy Astrophysics Science Archive Research Center (HEASARC), provided by NASAÕ's Goddard Space Flight Center.

REFERENCES

Andrews J. E. et al., 2010, ApJ, 715, 541
Andrews J. E. et al., 2011, ApJ, 731, 47
Arnett W. D., 1996, Supernovae and Nucleosynthesis. Princeton Univ. Press, Princeton, NJ
Arnett W. D., Bahcall J. N., Kirshner R. P., Woosley S. E., 1989, ARA&A, 27, 629
Balinskaia I. S., Bychkov K. V., Neizvestnyi S. I., 1980, A&A, 85, L19
Barbon R., Ciatti F., Rosino L., 1979, A&A, 72, 287
Baron E. et al., 2000, ApJ, 545, 444
Blondin S., Calkins M., 2007, Centr. Bureau Electron. Telegrams, 1119, 1
Botticella M. T. et al., 2009, MNRAS, 398, 1041
Branch D., Falk S. W., Uomoto A. K., Wills B. J., McCall M. L., Rybski P., 1981, ApJ, 244, 780
Branch D., Jeffery D. J., Blaylock M., Hatano K., 2000, PASP, 112, 217
Cappellaro E., Danziger I. J., Turatto M., 1995, MNRAS, 277, 10
Cappellaro E., Mazzali P. A., Benetti S., Danziger I. J., Turatto M., della Valle M., Patat F., 1997, A&A, 328, 203
Cardelli J. A., Clayton G. C., Mathis J. S., 1989, ApJ, 345, 245
Cernuschi F., Marsicano F., Codina S., 1967, Ann. d'Astrophys., 30, 1039
Chevalier R. A., 1982, ApJ, 258, 790
Chevalier R. A., 2008, in Hunt L. K., Madden S., Schneider R., eds, Proc. IAU Symp. 255, Low-Metallicity Star Formation: From the First Stars to Dwarf Galaxies. Cambridge Univ. Press, Cambridge, p. 175
Chevalier R. A., Fransson C., 1994, ApJ, 420, 268
Chugai N. N., Danziger I. J., 1994, MNRAS, 268, 173
Chugai N. N., Chevalier R. A., Utrobin V. P., 2007, ApJ, 662, 1136
Clocchiatti A. et al., 1996, AJ, 111, 1286
de Blok W. J. G., van der Hulst J. M., 1998, A&A, 335, 421
Dessart L., Hillier D. J., 2005, A&A, 437, 667
Dwek E., Galliano F., Jones A. P., 2007, ApJ, 662, 927
Elmhamdi A., Chugai N. N., Danziger I. J., 2003a, A&A, 404, 1077
Elmhamdi A. et al., 2003b, MNRAS, 338, 939
Ercolano B., Barlow M. J., Sugerman B. E. K., 2007, MNRAS, 375, 753
Fassia A., Meikle W. P. S., Geballe T. R., Walton N. A., Pollacco D. L., Rutten R. G. M., Tinney C., 1998, MNRAS, 299, 150
Fesen R. A. et al., 1999, AJ, 117, 725
Fox O. et al., 2009, ApJ, 691, 650
Fransson C., Chevalier R. A., 1987, ApJ, 322, L15
Fransson C., Chevalier R. A., 1989, ApJ, 343, 323
Fryer C. L., 1999, ApJ, 522, 41
Gerardy C. L., Fesen R. A., Höflich P., Wheeler J. C., 2000, AJ, 119, 2968
Gerardy C. L. et al., 2002, ApJ, 575, 1007
Hamuy M., 2003, ApJ, 582, 905
Harutyunyan A. H. et al., 2008, A&A, 488, 383
Heger A., Fryer C. L., Woosley S. E., Langer N., Hartmann D. H., 2003, ApJ, 591, 288

Hoyle F., Wickramasinghe N. C., 1970, Nat, 226, 62
Immler S., Brown P. J., 2007, Astron. Telegram, 1259, 1
Jeffery D. J., Branch D., 1990, in Wheeler J. C., Puran T., Weinberg S., eds, Jerusalem Winter School for Theoretical Physics: Supernovae, Vol. 6. World Scientific, Singapore, p. 149
Kasen D., Woosley S. E., 2009, ApJ, 703, 2205
Kotak R., Meikle P., van Dyk S. D., Höflich P. A., Mattila S., 2005, ApJ, 628, L123
Kotak R. et al., 2009, ApJ, 704, 306
Kozasa T., Hasegawa H., Nomoto K., 1991, A&A, 249, 474
Landolt A. U., 1992, AJ, 104, 340
Li W., Jha S., Filippenko A. V., Bloom J. S., Pooley D., Foley R. J., Perley D. A., 2006, PASP, 118, 37
Lucy E. et al., 1991, in Woosley S. E., ed., Supernovae. Springer-Verlag, New York, p. 82
Lucy L. B., Danziger I. J., Gouiffes C., Bouchet P., 1989, in Tenorio-Tagle G., Moles M., Melnick J., eds, Lect. Notes Phys. Vol. 350, Structure and Dynamics of the Interstellar Medium. Springer, Berlin, p. 164
McGaugh S. S., 1994, ApJ, 426, 135
Maguire K. et al., 2010, MNRAS, 404, 981
Mattila S. et al., 2008, MNRAS, 389, 141
Meikle W. P. S. et al., 2007, ApJ, 665, 608
Meikle P. et al., 2011, preprint (arXiv:1103.2885)
Mikuz H., Maticic S., 2007, Centr. Bureau Electron. Telegrams, 1116, 1
Moriya T., Tominaga N., Blinnikov S. I., Baklanov P. V., Sorokina E. I., 2011, MNRAS, 415, 199
Mould J. R. et al., 2000, ApJ, 529, 786
Nozawa T., Kozasa T., Umeda H., Maeda K., Nomoto K., 2003, ApJ, 598, 785
Nozawa T. et al., 2008, ApJ, 684, 1343
Pastorello A., 2003, PhD thesis, Univ. Padova
Pastorello A. et al., 2004, MNRAS, 347, 74
Pastorello A. et al., 2006, MNRAS, 370, 1752
Pastorello A. et al., 2009, MNRAS, 394, 2266
Patat F., Barbon R., Cappellaro E., Turatto M., 1994, A&A, 282, 731
Poole T. S. et al., 2008, MNRAS, 383, 627
Pooley D. et al., 2002, ApJ, 572, 932
Pozzo M., Meikle W. P. S., Fassia A., Geballe T., Lundqvist P., Chugai N. N., Sollerman J., 2004, MNRAS, 352, 457
Pozzo M. et al., 2006, MNRAS, 368, 1169
Pumo M. L. et al., 2009, ApJ, 705, L138
Pumo M. L., Zampieri L., Turatto M., 2010, Mem. Soc. Astron. Ital., 14, 123
Sakon I. et al., 2009, ApJ, 692, 546
Schlegel E. M., 1990, MNRAS, 244, 269
Schlegel D. J., Finkbeiner D. P., Davis M., 1998, ApJ, 500, 525
Schmidt B. P. et al., 1993, AJ, 105, 2236
Smartt S. J., Eldridge J. J., Crockett R. M., Maund J. R., 2009, MNRAS, 395, 1409
Smith N., Foley R. J., Filippenko A. V., 2008, ApJ, 680, 568
Smith N. et al., 2009, ApJ, 695, 1334
Smith N., Li W., Filippenko A. V., Chornock R., 2011, MNRAS, 412, 1522
Smoker J. V., Axon D. J., Davies R. D., 1999, A&A, 341, 725
Smoker J. V., Davies R. D., Axon D. J., Hummel E., 2000, A&A, 361, 19
Spyromilio J., Leibundgut B., 1996, MNRAS, 283, 89
Spyromilio J., Leibundgut B., Gilmozzi R., 2001, A&A, 376, 188
Suntzeff N. B., Bouchet P., 1990, AJ, 99, 650
Szalai T., Vinkó J., Balog Z., Gáspár A., Block M., Kiss L. L., 2011, A&A, 527, A61
Todini P., Ferrara A., 2001, MNRAS, 325, 726
Tully R. B., 1988, Nearby Galaxies Catalogue. Cambridge Univ. Press, Cambridge and New York, p. 221
Turatto M., Cappellaro E., Barbon R., della Valle M., Ortolani S., Rosino L., 1990, AJ, 100, 771
Turatto M., Benetti S., Cappellaro E., 2003, in Hillebrandt W., Leibundgut B., eds, ESO Astrophys. Symp. Vol. XVII, From Twilight to Highlight: the Physics of Supernovae. Springer, Berlin, p. 200
Utrobin V. P., 2004, Astron. Lett., 30, 293
Woosley S. E., Hartmann D., Pinto P. A., 1989, ApJ, 346, 395
Woosley S. E., Heger A., Weaver T. A., 2002, Rev. Modern Phys., 74, 1015
Zampieri L., 2002, in Cianci R., Collina R., Francaviglia M., Frè P., eds., 14th SIGRAV Conference on General Relativity and Gravitational Physics, Recent developments in general relativity. Springer, Milano
Zampieri L., 2007, in Antonelli L. A. et al., eds, AIP Conf. Proc. Vol. 924, The Multicolored Landscape of Compact Objects and Their Explosive Origins. Am. Inst. Phys., Melville, p. 358
Zampieri L., Pastorello A., Turatto M., Cappellaro E., Benetti S., Altavilla G., Mazzali P., Hamuy M., 2003, MNRAS, 338, 711

This paper has been typeset from a TEX/LATEX file prepared by the author.